A New Method for Continuous Posture Analysis Using Marker-based Video Processing Technique

Ramtin Nazerian

Submitted to the
Institute of Graduate Studies and Research
in partial fulfillment of the requirements for the degree of

Doctor of Philosophy
in
Industrial Engineering

Eastern Mediterranean University
June 2022
Gazimağusa, North Cyprus

Approval of the Institute of Graduate Studies and Research

Prof. Dr. Ali Hakan Ulusoy
Director

I certify that this thesis satisfies all the requirements as a thesis for the degree of Doctor of Philosophy in Industrial Engineering.

Prof. Dr. Gökhan İzbırak
Chair, Department of Industrial Engineering

We certify that we have read this thesis and that in our opinion it is fully adequate in scope and quality as a thesis for the degree of Doctor of Philosophy in Industrial Engineering.

Prof. Dr. Orhan Korhan
Supervisor

Examining Committee

1. Prof. Dr. Fethi Çalışır
2. Prof. Dr. Mahmut Ekşioğlu
3. Prof. Dr. Orhan Korhan
4. Assoc. Prof. Dr. Ender Angın
5. Assoc. Prof. Dr. Adham Makkieh

ABSTRACT

Many postural analysis techniques are developed to reduce the risk of musculoskeletal problems recently. Methods such as Rapid Entire Body Assessment (REBA) are capable of analyzing the static or awkward positions, but the selection of these postures is subjective. To make an objective postural analysis, devices such as Electro Magnetic Trackers (EMTs) can be used continuously during the job task, but utilizing such devices is costly. Other methods such as Red, Green, Blue, and Depth (RGB-D) cameras and Microsoft Kinect have also been used in multiple studies to continuously track human posture. However, the mentioned methods are only capable of representing a single joint angle for body segments. Therefore, in this study a cost-effective marker-based video processing algorithm is developed for measuring 3-Dimensional (3D) information regarding both the location and the orientation of human posture. The checkerboard pattern is selected as the markers to be detected in the video frame and relevant 3D location and orientation are calculated based on the Perspective n Point (PnP) approach. This study also investigates the precision of the measurements. Thus, an experiment was designed to capture markers in different known locations and orientations. Moreover, to validate the method of measurement, the second experiment is designed to compare the outcome of the proposed algorithm with the outcome of EMTs provided in another study. According to the result of the first experiment, overall, the algorithm was capable of measuring the 3D location and orientation of the markers with precision of 2.88 mm and 1.34° on average, respectively. Furthermore, the precision of the algorithm is found to be significantly affected by the marker pattern ($p < 0.001$). The higher the number of rows and columns showed a more precise measurement. The result achieved from the second experiment

shows no significant difference between the measured value of the algorithm and EMTs ($p = 0.880$). Although some of the limitations of the proposed algorithm such as undetectable checkerboards at extreme angles relative to the camera, and limited field of view of the camera, promising results are achieved with a low cost of implementation.

Keywords: 3d posture tracking, marker-based posture tracking, ergonomics, video processing, continuous posture analysis.

ÖZ

Günümüzde diye başlayabilirisin kas-iskelet sistemi sorunları riskini azaltmak için birçok postural değrlendirme yöntemleri geliştirilmiştir. Hızlı Tüm Vücut Değerlendirmesi (HTVD) gibi yöntemler, en sabit veya farklı pozisyonları analiz etme yeteneğine sahiptir, ancak bu duruşların seçimi özneldir. Objektif bir duruş analizi yapmak için Elektro Manyetik İzleyiciler (EMTr) gibi cihazlar iş görevi sırasında sıklıkla kullanılabilir, ancak bu tür cihazları kullanmak maliyetlidir. Kırmızı, Yeşil, Mavi ve Derinlik (RGB-D) kameraları ve Microsoft Kinect gibi diğer yöntemler de insan de insan postur analizi için birçok çalışmada kullanılmıştır. Bununla birlikte, bahsedilen yöntemler, vücut bölümleri için yalnızca tek bir eklem açısını temsil etme yeteneğine sahiptir. Bu nedenle, bu çalışmada, insan duruşunun hem konumu hem de yönelimi ile ilgili 3 Boyutlu (3B) bilgileri ölçmek için uygun maliyetli işaret tabanlı bir video işleme algoritması geliştirildi. Video karesinde algılanacak işaretçi olarak dama tahtası deseni seçilmiş ve perspektif n nokta yaklaşımına göre ilgili 3B konum ve yönlendirme hesaplandı. Bu çalışma aynı zamanda ölçümlerin kesinliğini de araştırmaktadır. Bu nedenle, bilinen farklı konumlarda ve yönlerde işaretleyicileri yakalamak için bir deney tasarlandı. Ayrıca, ölçüm yöntemini doğrulamak için ikinci deney, önerilen algoritmanın sonucunu başka bir çalışmada sağlanan EMT'lerin sonucuyla karşılaştırmak için tasarlanmıştır. İlk deneyin sonucuna göre, genel olarak, algoritma işaretçilerin 3B konumunu 2,88 mm hassasiyetle ve işaretçilerin 3B yönelimini ortalama 1,34° hassasiyetle ölçüldü. Ayrıca, algoritmanın kesinliğinin, işaretleyici deseninden önemli ölçüde etkilendiği bulundu ($p < 0,001$). Satır ve sütun sayısı ne kadar yüksek olursa, daha hassas bir ölçüm göstermiştir. İkinci deneyden elde edilen sonuç, algoritmanın ölçülen değeri ile EMT'ler arasında önemli bir fark

göstermemektedir ($p = 0.880$). Önerilen algoritmanın kameraya göre aşırı açılarda algılanamayan dama tahtası ve kameranın sınırlı görüş alanı gibi bazı sınırlamalarına rağmen, düşük bir uygulama maliyeti ile umut verici sonuçlar elde edilmektedir.

Anahtar kelimeler: 3B duruş takibi, işaretçi tabanlı duruş takibi, ergonomic, video işleme, sürekli duruş analizi.

DEDICATION

To the scientists who can benefit from this algorithm on their research

ACKNOWLEDGMENT

I would like to show my genuine appreciation to all the individuals who have helped throughout this research.

Firstly, I would like to express my sincere gratitude to the esteemed supervisor of mine, Prof. Dr. Orhan Korhan, for his generous support, practical feedback, and effective contributions on this research.

I would like to express my sincere thanks to the distinguished thesis monitoring members namely Assoc. Prof. Dr. Ender Angın and Assoc. Prof. Dr. Adham Makkieh for their time and efforts on providing suggestion and guidance during the progress of my thesis every semester. Their effective comments and inspiring support were significantly valuable to me.

Furthermore, I want to thank Prof. Dr. Gokhan İzbırak, the Chairman of the Department of Industrial Engineering for his continuous support and all lecturers who taught me during my studies.

Last but not least, I would like to thank my classmate, flow researcher, co-worker, and dear friend Dr. Ehsan Shakeri for his effort, and time devotion on this research.

TABLE OF CONTENTS

LIST OF TABLES

LIST OF FIGURES

LIST OF ABBREVIATIONS

2D	2-Dimensional
3D	3-Dimensional
A/P	Anteroposterior
AR	Axial Rotation
CNN	Convolutional Neural Network
CT	Computed Tomography
DF	Degrees of Freedom
EMTs	Electromagnetic Trackers
FPS	Frames Per Second
GPU	Graphical Processing Unit
H	Hypothesis
ISO	International Organization for Standardization
OC	Operating Characteristic
OCRA	Occupational Repetitive Action
OSHA	Occupational Safety and Health Administration
OWAS	Ovako working posture analysis system
PATH	Posture, Activity, Tools and Handling
PnP	Perspective-n-Point
Q-Q	Quantile-Quantile
REBA	Rapid Entire Body Assessment
RGB-D	Red, Green, Blue and Depth
RMSE	Root Mean Square Error
RULA	Rapid Upper Limb Assessment

SD	Standard Deviations
WBV	Whole-Body Vibration
WMSDs	Work-related Musculoskeletal Disorders

Chapter 1

INTRODUCTION

1.1 Background Study

The importance of human body posture and its impact on musculoskeletal health has been mentioned in several studies in recent decades (Baker & Mansfield, 2010; Grobler, Mostert, & Becker, 2018; Mani, Milosavljevic, & Sullivan, 2015; Nazerian, Korhan, & Shakeri, 2018; Pal & Dhara, 2018; Scaramuzza, Martinelli, & Siegwart, 2006; Sottimano et al., 2018; Wagner, Kirschweng, & Reed, 2009; Zhu et al., 2017). For instance, Grobler et al. (2018) investigated the impact of sitting versus stand-up posture among 123 sewing machine operators in four and a half years quantitative, retrospective, longitudinal study. His findings show a significant reduction in spinal injuries for the stand-up posture compared to the sitting posture.

Therefore, in order to evaluate body postures in a variety of conditions, many postural assessment techniques are investigated by researchers. Accordingly, many standards such as range of motion between the joints and overall body posture has been introduced through-out the literature (Buchholz et al., 1996; Hignett & McAtamney, 2000; McAtamney & Corlett, 1993). Quantification of body posture is a challenging problem and lack of accurate measurement can be observed in many of these techniques.

For example, Rapid Entire Body Assessment (REBA) technique uses still 2-Dimensional (2D) photos of the most awkward or prolonged positions to investigate the body segment angles. These angle measurements are estimated by the ergonomics experts. Furthermore, the selection of the critical posture in the above-mentioned technique is handled by the ergonomics expert as well. Therefore, both the selection and angle measurement of the body posture is vulnerable to human error.

1.2 Motivation to Solve the Problem

In order to compensate the subjective analysis, a method is required to continuously track the human posture and represent quantitative measurements for the targeted body segments. For this purpose, Electromagnetic Trackers (EMTs) are commonly used for tracking the human posture continuously using electromagnetic sensors. These devices are capable of representing 6 Degrees of Freedom (DF) information regarding the sensor 3-Dimensional (3D) location and orientation more than 30 times per second. By attaching these sensors to human body segments, the data represented by the EMTs can be used as a good interpretation of body segment position and orientations. Although such devices are perfectly capable of tackling the continuous human posture tracking, they are cost intensive and very hardware dependent.

Therefore, in this study, using computer vision, image and video processing techniques, and checkerboard patterns as trackers, an algorithm was developed to track human posture continuously as a lower cost and less hardware dependent alternative to EMTs.

1.3 Aims and Objectives

Two dimensional methods which are exposed to human error are applied in the literature. So, in order to close this gap in this field, this study considers an assessment

from 6 DF in 3D space. The main objective of this study is to represent 6 DF information, namely x y z location and x y z orientation in 3D space, for body joints continuously and with acceptable precision. The developed algorithm can both lower and the accessibility of postural tracking for future studies related to posture tracking and analysis. This technique can also be a useful utility for ergonomists and therapeutical practitioners for posture analyses in empirical cases of industry and clinical treatments, respectively.

1.4 Hypotheses

Throughout the study, validity and reliability experiments will be conducted to measure the accuracy and precision of the algorithm, and the following hypotheses will be tested.

Validity Hypothesis (H):

- There is evidence of significant differences between the data gathered using the developed algorithm and data measured using EMTs.

Reliability hypotheses:

- H1: The corner point pattern of checkerboards significantly affects the precision of orientation measurement.
- H2: The corner point pattern of checkerboards significantly affects the precision of location measurement.
- H3: The video resolution significantly affects the precision of orientation measurement.
- H4: The video resolution significantly affects the precision of location measurement.

- H5: The axes significantly affect the precision of orientation measurements.
- H6: The axes significantly affect the precision of location measurements.

1.5 Research Methodology

MATLAB version 2018b was employed to develop the algorithm in this research. This study uses checkerboard textures as markers that can be attached to different body sections for continuous 3D postural analyses. Then, using a Perspective-n-Point (PnP) problem approach, which is one of the methods that can determine the 6 DF information regarding an object in a perspective view, the algorithm detects corner points of the checkerboards in the images and returns the location and orientation of the board (Gao et al., 2003).

Since a video contains a chain of images (frames), the algorithm selects the frames one by one and analyzes them separately. Depending on the duration and frame rate of the video, the calculation time could vary significantly. In the following, explanations regarding the development of the algorithm and hardware specifications are demonstrated.

1.6 Structure of the Thesis

This thesis consists of 6 chapters with the first chapter being the introduction. In the second chapter a literature review of the previously relevant studies is discussed and literature gap are mentioned. To address the gap, in chapter 3 the method of the algorithm as well as validity and reliability are explained in details. Next, in chapter 4, relevant outcome of the studies is shown and appropriate statistical tests are demonstrated. A discussion chapter is provided after the fourth chapter to compare the achieved results with the results represented in the literature. Furthermore, limitations

of the studies are mentioned and possible future studies are revealed. Finally in the conclusion chapter significant findings their impacts are represented.

Chapter 2

LITERATURE REVIEW

2.1 Importance of Body Posture

In recent decades, many studies have mentioned the importance of human body posture and its impact on musculoskeletal health (Grobler et al., 2018; Pal & Dhara, 2018; Sottimano et al., 2018).

In a literature study conducted by Vieira and Kumar (2004), the importance of posture analysis is discussed extensively. In their research, the authors specifically focused on quantitative postural analyses. Their findings show the relationship between Work-related Musculoskeletal Disorders (WMSDs) and postural habits in variety of careers.

Zhu et al. (2017) developed an ergonomic job analysis tool to measure the necessary requirement for performing surgery while minimizing the needed instruction for the surgent in the operation room. In their study they used real time ErgoPART assessment tool to evaluate the common posture of surgent during the operation. ErgoPART is a software which was developed based on continues iteration of data collection about the operating process and the data which was transferred between ergonomic experts and medical staff during the process (Zhu et al., 2017). Similarly, Baker and Mansfield (2010) investigated the impact of Whole-Body Vibration (WBV) on standing posture among sixteen individuals. These individuals were instructed to perform a timed paged board task while being exposed to WBV as frequent as 4 Hz in the standing position.

Furthermore, Wagner et al. (2009) evaluated the postural behavior of automotive assembly operators based on investigating their foot placement. in order to pursue with their research, they used video recording technique to record 529 pickup and transporting task of workers in 32 assembly lines to measure the reaching angle, departure angle, hand or hands used for the task, handling height and forms of footpaths.

Kumar, Kumar, and Baliga (2013) conducted a cross sectional research on the prevalence of WMSDs among Indian dentists. They included 646 participants of the mentioned occupation in their study, and among their findings they stated a significant correlation between sustained work postures and reported musculoskeletal discomforts. These studies and many more are representing the importance of postural analysis in the ergonomics.

Therefore, in order to evaluate body postures in a variety of conditions, many postural assessment techniques are investigated by researchers in order to quantify different body positions.

2.2 Common Posture Analysis Methods

REBA, Rapid Upper Limb Assessment (RULA), the Ovako Working Posture Analysis System (OWAS), Posture, Activity, Tools and Handling (PATH) and Occupational Repetitive Action (OCRA) are some of the assessment techniques for postural analysis (Buchholz et al., 1996; Hignett & McAtamney, 2000; Karhu, Kansi, & Kuorinka, 1977; McAtamney & Corlett, 1993; Occhipinti & Colombini, 1996; Pillastrini et al., 2010).

Al Madani and Dababneh (2016) have represented an extensive literature-based study on REBA. In their study, they emphasized on the conveniency and robustness of the tool, and they have also investigated the validity of the method by mentioning studies which compared the result of REBA with other observational and direct methods. Similar to REBA, RULA is another common tool for posture analysis which has been extensively used in studies where the upper bodies posture plays and important role. For instance, Golchha et al. (2014) used this technique to analyze the upper body posture of 104 dentists in India. Moreover, Dockrell et al. (2012) assess the body posture of 24 school children while they were using computers. Additionally, Namwongsa et al. (2018) investigated the body posture of 30 smart phone users using RULA technique.

Even though many of these assessments are being utilized frequently for postural analysis in many research studies, they are limited to instances of time when the most awkward or prolonged positions happen (Hignett & McAtamney, 2000; Nazerian, 2016). In order to take into account every instance of a job task, observations are required to be video recorded and every frame needs to be assessed separately. In order to be more specific, Brodie and Wells (1997) emphasized on the unreliability of some posture analysis techniques such as RULA, and Occupational Safety and Health Administration (OSHA) upper limb and lower back stress analyses check list (Vieira & Kumar, 2004). Furthermore, Vieira and Kumar (2004) point out the unreliability, bias effect of the ergonomic expert opinion, low precision measurement of body segments, and the extended time of analyses as the disadvantage of commonly used qualitative postural analysis methods.

2.3 Continuous Postural Analysis

Assessment of every video frame for postural analysis is very time consuming; moreover, the likelihood of measurement errors should be taken into account.

Many researchers applied new techniques to keep track of the location and orientation of body parts automatically (Balaraman et al., 2018; Bhatt & Skm, 2018; Buzzi et al., 2017; Masaki et al., 2018; Nguyen et al., 2018; Perera et al., 2016; Suzuki et al., 2019). Techniques and utilities such as body area network sensors, Electromagnetic Trackers (EMTs), and Optical posture tracking are commonly used in variety of studies for the purpose of continues posture tracking.

In order to be more specific, Lemmers et al. (2018) used EMTs to measure the 3D kinematic of active lateral bending and flexion-extension movement of 35 participants with non-specific neck pain as well as 100 individuals as the control group. Furthermore, Hoppes et al. (2018) studied 15 patients suffering from visual vertigo in virtual reality environment. In their research they utilized EMT to track and record the position of the participants' head and center of the mass during the experiment. Moreover, Gascon et al. (2018) investigated the effect of different garment on the position of the scapular kinematic of 40 females. They measured the scapula 3D position, these researchers used EMT as well. These approaches help the researchers in the field of ergonomics to measure body posture continuously, faster and more precisely.

2.3.1 Body Area Network

One of the devices used to represent the body posture of an individual is body area network. This device take advantage of accelerometer and gyroscope sensors to

represent acceleration and orientation of a specific body segment after attachment (Sivanathan, 2014).

Valero et al. (2017) developed a robust system to illustrate motion-related information for posture and biomechanical analysis of the individual's body using body area network sensors. In their study, the used construction trade workers as their subject and participants were asked to perform bricklaying activity while 8 sensors attached to their body segment. The authors introduced 16 primary body positions in their system and these positions were represented simultaneously as the workers were performing the task. The method emphasizes specifically on the intuitive and easy to understand information related to posture analysis.

Apart from representing and in-depth review about the postural investigations for constructional workers, Valero et al. (2016) utilized their developed software for the purpose of posture analysis of material handling among construction workers using body area network sensors. In their study they concluded that the current practice of posture analysis in construction industry is mostly based on visual representation which lacks the precision and accuracy requirement of assessment. Therefore, taking advantage of electronic based devices such as body area network is necessary for more reliable postural assessment.

Dong et al. (2015) also used the body area network sensors to assess the kinematic data related to patients who are suffering from Parkinson's disease. This research focused on understanding the environmental location and activity specifications when freezing of gait happens in these patients. Freezing of gait is a disability where briefly people with Parkinson's disease lack the ability to perfume the stepping task for a short

period of time (Nutt et al., 2011). Dong et al. (2015) attached 6 sensors on chest, wrists, hips, and ankles of the patients and asked them to perform basic tasks such as walking, sitting, and lying down. Similarly, they measured the same actions using healthy individuals for the purpose of data comparison.

Although body area network device is capable of representing data related to acceleration and orientation of the body segments, the 3D coordinates and rotation of these body segments cannot be measured (Valero et al., 2017).

2.3.2 EMTs Application

EMTs are one of the most commonly used devices in continuous postural analysis techniques. These devices consist of several electromagnetic sensors and a source. Each sensor represents its 3D coordinate and orientation relative to the source, and therefore, by attaching these sensors to the targeted body parts, the location and orientation of the body parts can be estimated in 3D space. EMTs are capable of representing 6 DF information, which are x, y, z values and x, y, z Euclidean angles, up to approximately 240 times per second with an accuracy of 0.8mm for location and 0.15° for orientation (Balaraman et al., 2018). While EMTs are very accurate for 3D pose estimation, based on the literature, they are costly and less common among non-clinical studies such as ergonomics studies.

Suzuki et al. (2019) used EMTs to investigate the effect of thoracic position on scapulothoracic and glenohumeral activities during eccentric shoulder external rotation. Moreover, Habechian et al. (2016) used the same device to examine the gender-specific differences of scapular kinematics during arm elevation among children and adults. Likewise, Learman et al. (2016) studied the trunk reposition error of individuals with acute stroke using EMTs.

In a study conducted by Geisbüsch et al. (2017) the application of EMT was investigated for the purpose of de-rotation angle measurement in adults with internal rotation gait diagnosis. The authors compared EMT measurement for de-rotation with the traditional method of using Computed Tomography (CT) scan. In their experiment they attached the EMT to the patient pre, under, and post-surgery for the purpose of measurement. Then after, the compared the deviation of pre, and post-surgery measurements with the result of the CT scan as the reference. Their finding shows a precise measurement with deviation of only 2.6 degrees. The purpose of this study was to find a better alternative measurement device than using CT scan to limit the exposure to radiation.

Recently, Geisbüsch et al. (2021) used EMTs for femoral de-rotation osteotomy operation. The device was utilized to dynamically monitor the angle of de-orientation during the surgery. Before the surgery basic measurements was done using CT scan and MRI, and after the rehabilitation period postoperative gait analysis was done on the patients to measure the static changes of the operation.

Woodburn et al. (1999) used EMTs for 3D measurement of the kinematic specification of angle joint complex. In their study, ten participants who were suffering from rheumatoid arthritis and joint angle instability and deformability were selected for their experiment. Moreover, ten more healthy participants with no record of musculoskeletal diseases or trauma in the lower limb or feet were selected for the control group. Both groups were undertaken the gait analysis and promising data was achieved in comparison with several published studies (Kobayashi et al., 1997; Moseley et al., 1996; Rattanaprasert et al., 1999).

Another study conducted by Woodburn, Helliwell, and Barker (2003) took advantage of EMTs to assess the effectiveness of custom foot orthoses for the individuals who are struggling with rheumatoid arthritis. Using EMTs on the ankle joint complex, 3D kinematic information was recorded for a period of 30 months and compared with healthy people with no issue in their feet. They stated the effectiveness of continuous use of foot orthoses for the deformity correction and functionality optimization of joint ankle complex among these patients.

Since EMTs can be produce in small form factor, a study conducted by Kellermeier et al. (2017) used these small sensors for the purpose of clinical evaluation study on catheter navigation in interstitial high dose rate brachytherapy. The utilization of EMTs achieved the maneuver precision with the range of 0.17 up to 0.13 mm depending on the type of table the task was performed.

The application of EMTs is not solely limited to ergonomics and clinical based studies. In fact, these sensors are found to be useful in the sports industry as well. Cerrito et al. (2018) investigated the kinematic behavior of cervical spine of rugby players while performing union scrumming. The study was designed to specifically test the reliability of measurements using interclass correlation coefficient, standard error of measurement, and minimum detectable change. Results shows promising precision of measurement for utilizing this device for the purpose.

Being capable of representing 6 DF of information, EMTs have the variety of usages in the field of posture tracking. However, considering the cost and accessibility of the device, many researchers look for other cheaper and more accessible alternatives for their experiments.

2.3.3 Optical Posture Tracking

Another common method recently used for 3D postural tracking is optical tracking also known as kinematics computer vision (Buzzi et al., 2017; Dang et al., 2017; Jones et al., 2016; Wang et al., 2018; Xu & McGorry, 2015). Utilizing computer vision techniques to recognize a 3D object has recently gain popularity in many industries. In order to fully grasp an understanding about the computer vision the following definition is quoted:

> Computer vision is the science and technology of making machines that see. It is concerned with the theory, design and implementation of algorithms that can automatically process visual data to recognize objects, track and recover their shape and spatial layout (Cipolla, Battiato, & Farinella, 2010, p. VII).

In their book the divided the concept of vision in to two main frame works. A photometric framework which is the reconstruction of an image on a 2D Euclidean plane, and a special frame work which focuses on the configuration of a shape, possibility of displacement and 3D special features (Cipolla et al., 2010).

Transition between these two frameworks, although challenging, have many applications in different sciences and industries such as physics, robotic, health science and art. Thanks to light-sensitive crystals in photographic films as well as charge-couple device, active pixel sensor and metal-oxide-semiconductors transistors in digital camera sensors, nowadays projection of 3D objects can be recorded as 2D image in a fraction of time (Janesick, 2001; Keller et al., 2000). On the other hand, reconstructing the information of a 3D object from a 2D image has many challenges to be overcame. When transition from a 3D space (object) to a 2D space (image) information related to the depth will be lost; and therefore, retrieving the information requires further computation and analysis.

One way to address the issue is to use the triangulation technique. In this respect, an object depth can be calculated from two images taken from the object with different points of view. It should be mentioned that, the points of view or the distance, and the orientation between them should be a known factor to do the calculation (Hartley & Sturm, 1995). The application of stereo or multiple camera posture tracking is available in many studies which is discussed in more details later on this chapter. (Liu, Han, & Lee, 2016; Pellegrini & Iocchi, 2007).

The basic concept of triangulation in a 2D plane is demonstrated in Figure 1. Given the information about positions, orientations, and angles of view of the camera 1 and 2 in the mentioned figure, the angles of α and β can be calculate.

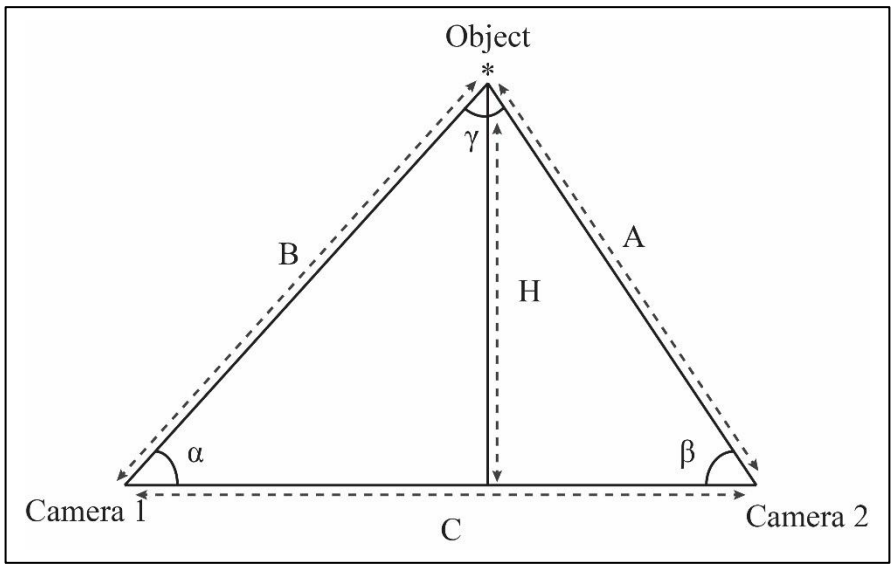

Figure 1: Triangulation for 3D Object Detection

Let's consider (x, y) coordinates as the position of camera 1 and (x′, y′) coordinates of camera 2. In order to calculate the distance between two cameras, Euclidean distance equation is used (Guichard et al., 2020). Considering the known α and β angles, ɣ can be calculated using Equation 2. Next with known α, β, and ɣ angles as well as C, the

opposite side of each angle can be calculated using the law of signs (Beveridge, 2014). Accordingly, equation 3 is demonstrated. Finally, the distance of the object H perpendicular to line between camera 1 and camera 2 can be calculated using equation four.

$$C = \sqrt{(x - x')^2 + (y - y')^2} \tag{1}$$

$$\gamma = 180 - (\alpha + \beta) \tag{2}$$

$$\frac{A}{\sin\alpha} = \frac{B}{\sin\beta} = \frac{C}{\sin\gamma} \tag{3}$$

$$H = A \times \sin(\beta) = B \times \sin(\alpha) \tag{4}$$

Although the above-mentioned calculations are seemed to be accurate and requires low amount of computation in 2D, expanding it to the 3D world introduces many challenges. For instance, measuring the camera location and orientation in 3D space is difficult and exposed to many errors. Moreover, having a clear reading of the image of the object from the camera sensor and image distortions in variety of camera lenses can introduce many issues for estimating the angle of the object relative to the camera (Hartley & Sturm, 1997). In order to address image distortion issue, Hartley and Sturm (1997) considered a Gaussian noise in the coordinates of the images and attempt to minimize the square error for the estimation. Furthermore, to solve the sensitivity to proper initialization, nonlinearity, and spatial distribution of the special points also known as world points cloud, Alsadik (2016) introduced a modified solution for the 3D triangulation problem using inclined angles which were calculated based on the image coordinate systems as well as spherical trigonometry rules and vector geometry. With all the above-mentioned approaches to resolve the complexity of stereo or multi-camera triangulation, precise measurements of the orientation and location of the cameras play significant role on the precision of the 3D demonstration.

The other way to estimate the depth information of a 2D image is to use PnP. With known location of some known 3D location of selected world points as well as their equivalent image point coordinates, PnP methos is capable of determining both the location and orientation of the camera relevant to the points(Youyang et al., 2019). Determining the coordinates and the orientations of camera relative to an object solely does not satisfy the purpose of postural tracking. However, when the relative coordinates and orientations are determined, the basis of the coordinate system can be changed to put the camera in the basis and the object in the perspective of the camera. This feature, was selected for this study specifically since compared to stereo vision technique, the number of cameras required to follow with the procedure of postural tracking reduces to only one which accordingly would make the system less hardware intensive.

The PnP uses equation five as the main structure of the concept.

$$s_i \begin{bmatrix} u'_i \\ v'_i \\ 1 \end{bmatrix} = \begin{bmatrix} r_{11} & r_{12} & r_{13} & t_1 \\ r_{21} & r_{22} & r_{23} & t_2 \\ r_{31} & r_{32} & r_{33} & t_3 \end{bmatrix} \begin{bmatrix} X_i \\ Y_i \\ Z_i \\ 1 \end{bmatrix} \tag{5}$$

Where u'_i and v'_i are the pixel coordinates of image point i, X_i, Y_i, and Z_i are the 3D world coordinates of point i, and s_i is the scale factor of the picture (if any). The 3×4 matrix in the equation are the 12 unknown variables that need to be determined to represent the transformation matrix for the location and orientation of the camera (Youyang et al., 2019). Given the fact that equation 5 does not consider the camera specifications including the focal length and principal point of the camera, a third matrix can be inserted in the equation 5 to represent (see equation 6) (Hartley & Zisserman, 2003).

$$s_i \begin{bmatrix} u_i' \\ v_i' \\ 1 \end{bmatrix} = \begin{bmatrix} f_x & \gamma & u_0 \\ 0 & f_y & v_0 \\ 0 & 0 & 1 \end{bmatrix} \begin{bmatrix} r_{11} & r_{12} & r_{13} & t_1 \\ r_{21} & r_{22} & r_{23} & t_2 \\ r_{31} & r_{32} & r_{33} & t_3 \end{bmatrix} \begin{bmatrix} X_i \\ Y_i \\ Z_i \\ 1 \end{bmatrix} \quad (6)$$

Where f_x and f_y are the focal length of the camera based on the lens, γ is the skew factor which in case of absence would be set to zero, and u_0 and v_0 are the principal point of the image sensor. the camera parameter mentioned in equation 6 usually are pre-determined using various camera calibration techniques (Hartley & Zisserman, 2003).With known camera parameters, 3D coordinates of a world point, and its relative image coordinates, 12 unknown variables are remained undetermined. Equation 6 can be transformed into 3 homogenous linear equation with mentioned 12 unknown variables. Therefore, at least 4 points are required to determine the variables. After determining the variables r_{11}, r_{12}, r_{13}, ..., r_{33} as well as t_1, t_2, and t_3. they can be interpreted as the 3D transformation matrix of the camera where r_{ij} *for i = 1. 2, and 3,* and *j = 1, 2, and 3* represent the 3D rotation matrix and t_i *for i = 1, 2, and 3* represent the 3D coordinates of the camera (Bar-Itzhack, 2000).

Even though determining the object location and orientation using PnP is not depend on very advanced measurement devices, existence of noise and unsureness about the true location of both world points and camera point is causing the calculation to be vulnerable to some degree of uncertainty. In order to compensate for this issue, techniques such as Random Sample Consensus introduced by Fischler and Bolles (1981) are utilized for 3D location and orientation estimation. Similarly, Youyang et al. (2019) has address the issue of none-scaled measurements through 3D axes of the world point. In order to eliminate this effect, Youyang et al. (2019) suggested a normalized technique to make the *X*, *Y*, and *Z* axes values on the same scale. According

to their findings, significant improvement is achieved on estimating the correct location and orientation of the object after normalization.

Recently, Seo et al. (2019) investigated three different motion capture approaches for postural analysis. Accordingly, they have categorized these approaches: (a) Red, Green, Blue and Depth (RGB-D) sensor-based approach (Han et al., 2013); (b) stereo-vision camera-based approach (Starbuck et al., 2014); (c) multiple camera-based approach (Alwasel et al., 2013).

A study conducted by Abobakr et al. (2017) used the combination of Kinect RGB-D sensor and convolutional deep neural network to predict 29 joint angles based on the RULA method. In their study, they generated two hundred thousand images using 3D human models, initially captured from a participant doing assembly procedure, for their convolutional neural network model. To represent the model as an input data, they used a 3 layer of RGB for every pixel with the color representing the depth information. Their findings show root mean square error of 6.64 ± 2.73 degrees. It should be mentioned that the estimated angles from their models is specifically related to those required in RULA method and the Euclidian 3D angles are not represented. Later on, the study was published with higher accuracy of angle measurements, as well as 89% RULA score accuracy (Abobakr et al., 2019).

The RGB-D tools is not limited to posture tracking for ergonomics purposes. Khosrowpour et al. (2014) used the RGB-D sensors to classify actions of indoor construction workers based on their body poses. The main application of their research was to identify possible bottle necks in the work process of the targeted occupation as well as analyzing and assessing the workers productivity in the job. For this reason,

they used kernel density estimation technique to classify bag of poses based on the series of RGB-D data captured in the work environment. Their model consists of poses such as walking, measuring, idling picking up, and putting down in the timeline of the job task. Their clustering algorithm detects the mentioned poses during the timeline automatically to represent the overall activity summary of a job task with 81% accuracy.

In order to test the validity and accuracy of using RGB-D sensors for the purpose of action classification in construction workers, Han et al. (2013) conducted a comparative study between RGB-D sensors and more accurate marker-based motion recording device. In their study, they considered the data received from the marker-based device as the ground truth and assessed the measurement offsets of the RGB-D sensors accordingly. Their findings show 10.7 Cm and 16.2 degrees deviation from the ground truth in the location and angle measurement, respectively. However, they stated that such discrepancy in the measurement is not concerning for its purposed job in construction industry.

In order to expand the application of RGB-D sensors even further, Patruno et al. (2019) developed a method to utilize the sensor for the re-identification purposes based on the subject posture. They considered skeleton standard posture to create specific signatures for people's biometric body postures. It should be mentioned that, using RGB-D for this purpose is not solely investigated in the mentioned study, and other researchers have assessed the method as well (Ahmed, Jones, & Marks, 2015; Ren et al., 2017; Schumann & Stiefelhagen, 2017).

Seo et al. (2019) described the RGB-D approach as sensitive to sunlight and suitable for an indoor environment. This device is equipped with an infrared sensor and is able to provide the depth information of the 2D images. Moreover, the stereovision camera-based approach uses two cameras to extract point clouds of similar images from two different angles of view. Using triangulation, the method calculates 3D locations of the point clouds and, consequently, computes optical depth information. On the other hand, the multiple camera-based technique is less hardware dependent, can be applied using ordinary cameras and is suitable for an outdoor environment. The drawback of this method is the calculation time for estimating body joint angles.

Other than RGB-D technique, stereo vision has also been utilized in several studies for the purpose of postural tracking. For instance, Starbuck et al. (2014) raise the issue of sunlight and existed heat in the construction sites for postural tracking of the construction workers. Since the RGB-D cameras use infra-red signals to track human posture, they are not a good fit when it comes to long distance tracking and outdoor environment where the sun hit interfere with cameras' sensor. Thus, to solve the problem, they suggested utilizing stereo camera vision instead to cover bigger area for tracking and eliminate the outdoor limitation of RGB-D. In their study they suggested the usage of currently existing 3D kinematic tracking systems for such environment. Moreover, in a study conducted by Lee & Park (2019), stereo camera vision was used to track not only single but also multiple construction workers within the site. In order to track each worker separately, rather than using specific postural feature, they utilized entity tracking procedure which uses workers position and direction of movement across multiple cameras differentiate each person from their workmate.

According to their findings, their method is capable of capturing 96% of actual movements within 0.8-meter error in estimation of their location.

In order to monitor and prevent occupational accidents and injuries, Liu et al. (2016) developed a close to real time 3D skeleton feature extraction algorithm by two streaming cameras. Basically, instead of locating the 3D joint location of the participants, their algorithm tracks the body joints in one camera steam through successive frames and then identify the tracked joints in the secondary stream to construct the 3D motion of the skeleton joints. In their study they stated that, their algorithm is capable of being utilized in construction sites and it also requires two smartphones for video capturing.

Apart from the ergonomics application of the stereo vision technique, many studies used the method for robotic and even surgical instrument navigation. As an example, a research done by Zhou et al. (2017) used the stereo vision technique to navigate common and/or small sized instruments used in surgeries to track the device in 3D space for a better and more precise application. In their approach, they installed infrared LEDs on the instruments as the marker as well as near infrared filters in front of the stereo camera lenses to track the instruments. It should be mentioned that the study was developed using simulation techniques. According to their findings, high stability and precision is achievable with this technique.

Throughout the literature search, no study was found to use PnP approach for postural tracking in ergonomics field. Since this approach has the potential to provide 3D rotation and orientation, this study has used it to provide a new algorithm accordingly.

Even though all three approaches are known as marker-less optical trackers that reduce interference for postural analysis, they can only estimate a single angle for joint position. Consequently, when it comes to joints with more than one axis of rotation, such as the hips and shoulders, these optical methods are not suitable (Seo et al., 2019).

2.4 Research Contribution

According to the information provided in this literature, techniques that are commonly used in the continuous posture analysis include digital inclinometers, Body Area Network, RGB-D, and EMTs have some limitations individually.

Attaching digital inclinometers on the human body is very challenging and in order to measure different joint orientation of a subject it may require multiple inclinometer attachments at different locations around the target joint. Moreover, Body Area Network ad RGB-D techniques are capable of tracking the human posture continuously and instantly. The RGB-D method also has the advantage of being marker-less approach to track the posture which reduces the job interference significantly. However, if the intended analysis requires 6 DF information regarding a body joint, both methods cannot provide such information. On the other hand, EMTs not only are capable of providing information regarding 3D location, but also 3D orientation of the targeted muscle. Although this feature makes the EMTs the best candidate to be used in continuous posture analysis with 6 DF information as requirement, they are expensive and, in many cases, where the budget of assessment is insufficient, other alternatives would be considered.

Based on the aforementioned literature, for continuous body posture analyses, methods are either cost intensive or lack 6 DF information regarding the 3D position (Dartt et

al., 2009; Gold et al., 2012; Jackson, Mathiassen, & Liv, 2016; Plamondon et al., 2007; Rezagholi, Mathiassen, & Liv, 2012). According to the literature, no previous study was found that uses a video processing algorithm which continuously assess 3D coordinate estimate and orientation of the body joints using a camera.

Chapter 3

METHODOLOGY

Given the fact that common continuous posture tracking methods either very costly to be used or are not capable of representing 6 DF information about the location and orientation of the body segments, this study aims to develop an algorithm to overcome both measurement errors and time consumption for continuous postural analysis; meanwhile, cost-effectiveness and minor hardware dependency have been considered throughout this study in order to make the approach easier than current methods for further research studies. MATLAB (2018b) software was employed to develop the algorithm in this research. Furthermore, this study uses checkerboard textures as markers which can be attached to different body sections for continuous 3D postural analyses. Then after, by using Perspective n Point (PnP) problem approach, which is one of the methods that can determine the 6 DF information regarding an object in perspective view, the algorithm detects corner points of the checkerboards in the images and returns the location and orientation of the board (Gao et al., 2003).

Since video contains a chain of images (frames), the algorithm selects the frames one by one and analyzes them separately. Depending on the duration and frame rate of the video the calculation time could vary significantly. In the following, explanations regarding the development of the algorithm and hardware specifications are demonstrated.

3.1 Checkerboard Preparation

Given the fact that the algorithm is based on PnP calculation, using a checkerboard pattern as the marker includes many advantages. Checkerboard pattern are easy to be produced. To be more specific, generating such patterns can be easily handled by using tables in MS Word and setting the row and column sizes to the desired dimensions. Then, every other cell of the table in black the checkerboard pattern was printed using a black and white printing device. Moreover, it is common to look for intersection points in an image where there is a high amount of contrast in the image. This point in fact is described as the corner points in this research. It is a good practice to measure the size of the squares after they being printed to make sure they are not rectangle due to the printing setting and represent the intended dimension as was set up in the computer.

The corner points detected in the frames are actually the inner corner points. Therefore, from now on, we will represent the number of corner points by the number of inner points in rows and columns. It should be mentioned that the combination of the points is supposed to be odds in rows and even in columns or vice versa in order to be 360° asymmetric. Figure 2 emphasizes more about the importance of board properties.

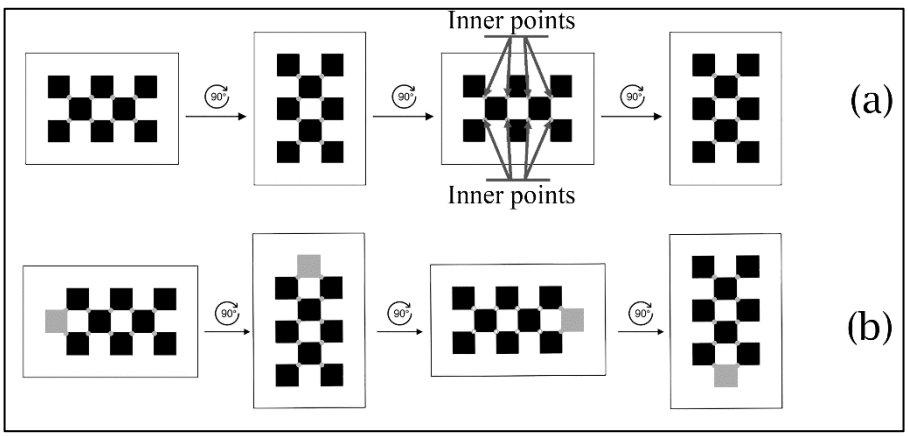

Figure 2: Checkerboard Properties

Figure 2 illustrates that a combination two by four corner points which leads to symmetricity of the shape for rotations more than 90°. From left to write checkerboards first and third, as well as, second and fourth are similar respectively, even though it has been rotated by 180°. Also, a combination of two by five corner points which does reveal an asymmetric feature to the board (marked with gray color). This property leads to rotational uniqueness from 0° to 360°. (Note) The gray circle markers show the corner points detected by the algorithm.

In order to emphasize more on the concept of symmetricity, in figure 2 part a 3 by 5 checkerboard pattern is represented. Accordingly, from left to right after rotating the checkerboard by two 90 degrees, similar pattern can be achieved. This means that at each instance of the measurement, there are two solutions for the orientation of the checkerboard which are 180 degrees apart. In order to eliminate this uncertainty, considering the patterns of combination of odd and even rows and columns such as, 3 by 4, 3 by 6, or 5 by 6 is recommended.

The size and the number of the corner points in each checkerboard pattern my play a significant role on the precision of the measurement. As discussed in the literature chapter, in order to solve the PnP problem, at least 12 points should be selected. However, considering the uncertainty of exact location of the corner points due to subpixel estimations and noises, it is recommended to select the pattern with higher number of corner points to limit the unwanted factors on the measurement. On the other hand, having a small size of squares concentrate all the selected points in to the certain region of the image and depending on the distance of the checkerboards from the camera, less precise location of the corner points is expected. Therefore, to have a better estimation of the corner points in the image, it is a good practice to provide

patterns with bigger square size to cover further distances. With all of that being mentioned, bigger square size and more corner points require more occupied space for the markers and this expansion is feasible up to a certain pattern. In order to investigate the relationship between the checkerboard pattern and the precision of the measurement, an experiment is designed which is explained in detail further in this chapter.

In order to attach these checkerboards in different body sections, the checkerboards were printed and attached to a hard thin polystyrene panel by glue. The reason to select this material is to making sure that the patterns are flattened correctly and are not warped. Furthermore, polystyrene is light weight and is a good candidate for the practical usage of this technique. The panel was attached to an elastic strap and was glued by a small piece of panel behind as the support. The purpose of using elastic straps is for making sure that they will put pressure equally around the body surface such that it would not block the blood flow or causes any discomfort to the participant, while fixes the panel firmly to reduce the noise due to body movements. Moreover, the elastic bands are adjustable for different body parts and sizes. After the preparation of these markers, they will be attached to locations of interest in order to be detected on the image and thus 6 DF information about the targeted joints can be calculated accordingly.

3.2 Camera Preparation

A smart phone video camera capable of recording videos with pixel resolution of up to 4000×3000 at 24 Frames Per Second (FPS) or up to 1920×1080 at 120 FPS, physical sensor size of 51×68 mm, and the focal length of 3.99 mm, is used for this study. However, each camera has its own specifications which for the accuracy of the results

must be taken into account. These specifications are mainly the focal length of the lens, the amount of distortion due to curvature of the camera lens, resolution, frame rate, aperture, shutter speed and International Organization for Standardization (ISO) value. ISO is the shortened term of ISO 5800:1987 commonly used to mention the sensitivity of the camera sensor to the light coming through the lens ("ISO 5800:1987(en) Photography — Colour negative films for still photography — Determination of ISO speed.," 2016; Thai, Cogranne, & Retraint, 2013).

There are three variables which are controlling the amount of exposure to the sensor of the camera. Shutter speed, ISO value, and the aperture can control the amount of light hitting the sensor of the camera. Other than the exposure, each one of these factors play an important role in the checkerboard detection and the precision at which the corner points will be detected.

In order to estimate the 3D location an orientation of an object using PnP problem, given the projected points on a 2D image, relevant cloud points with correct scales need to be presented in 3D space. This cloud points are called world points (Li, Xu, & Xie, 2012). For the first two specifications, MATLAB version 2018b software includes an application which not only calculates the focal length of the camera and distortion using a checkerboard pattern, but also is able to generate world point cloud of checkerboard corners in 3D space given the size of the checkerboard squares(Fu, 2004; Heikkila & Silven, 1997; MATLAB, 2017; Scaramuzza et al., 2006; Urban, Leitloff, & Hinz, 2015).

Shutter speed which controls the amount of time the sensor is exposed to the scene per each frame can limit the amount of time the camera receives light. The higher the value

of the shutter speed, the darker the image gets. Depending on the light available in the scene, the shutter speed will be adjusted to set the correct exposure of the frame. Although low shutter speed can make an image brighter, while the shutter is open in front of the sensor, any motion happening can cause a blurry image being captured for the frame which is called motion blur. To demonstrate the effect of motion blur in an example, figure 3 is provided.

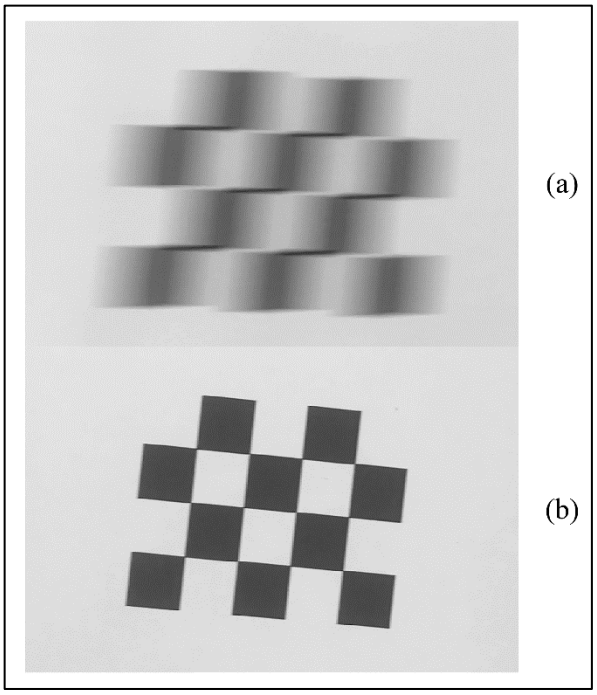

Figure 3: Sharpness of the Frames with Different Shutter Speeds

In figure 3, a checkerboard was captured while having a horizontal motion in front of the camera sensor. In part (a), the camera shutter speed was set to one thirtieth of a second which means that the shutter of the camera was open for 3.3 milliseconds. This has caused the motion blur to be occurred in the capture frame. On the other hand, on part (b) the same movement was capture but with the shutter speed of one two hundredth of a second. With the faster shutter speed close to no motion blur was introduced while capturing the frame. Clearly, detecting the corner points in the part

(b) is more precise than part (a). It should be mentioned that, for part (b) more intense lighting was used to capture the motion in order to have the same exposure of the checker board compared to part (a).

Another factor that plays an important point in the precision of the corner point detection is the ISO value. ISO can be considered as an amplification of the signal sent from the camera sensor after receiving the light through the camera lens. Each pixel of the camera sensor sends an electricity current to demonstrate the amount of brightness of the relevant image pixel. Sometimes, due to low light condition, an amplification of the signal is required to capture the pixel exposure correctly. Hence, the higher the amplification or the ISO value, the brighter the image gets. However, increasing the ISO value introduces some artifacts named salt and pepper noise. In order to observe such artifacts, Figure 4 is demonstrated.

In figure 4 part (a) the image was captured at ISO of 12800 while in part (b) the ISO was set to the lowest value of 100. As can be seen, there are many noises introduced to the image captured in part (a). These noises are produced as some image pixels representing the wrong value due to the amplification of the signal. In order to reduce the camera ISO value, more intense light is required to capture the image with the right exposure.

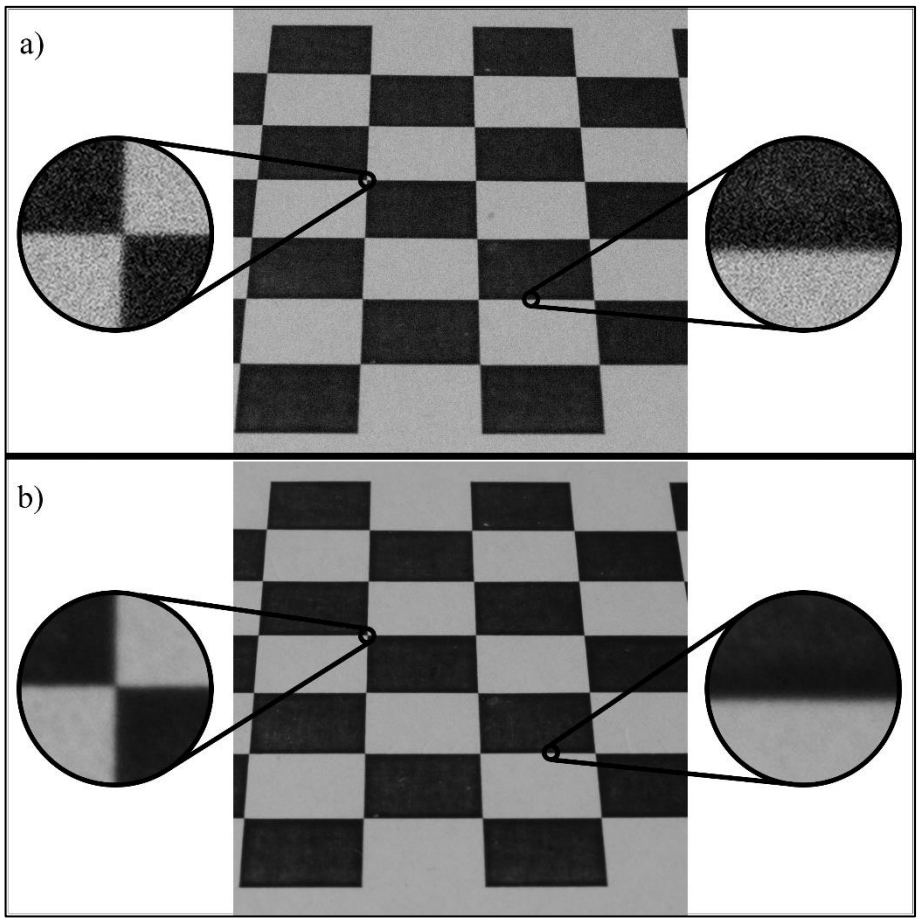

Figure 4: The Effect of ISO on Clarity

Last but not least, aperture is the other factor affecting the exposure of the image. Aperture is a variable gate located in the camera lens and is capable of controlling the amount of light that passes through from the lens to the camera sensor. Usually, the mechanism consists of several blades that are arranged in a circular pattern to act as circular gate with variable diameter. Increasing and decreasing the diameter of the aperture increases and decreases the amount of light passing through the lens, respectively. However, the bigger the size of the aperture, the shallower the depth field gets. The depth of field is the depth at which the capture image is in focus. In order to demonstrate the effect of aperture in the focus depth of an image figure 5 is provided.

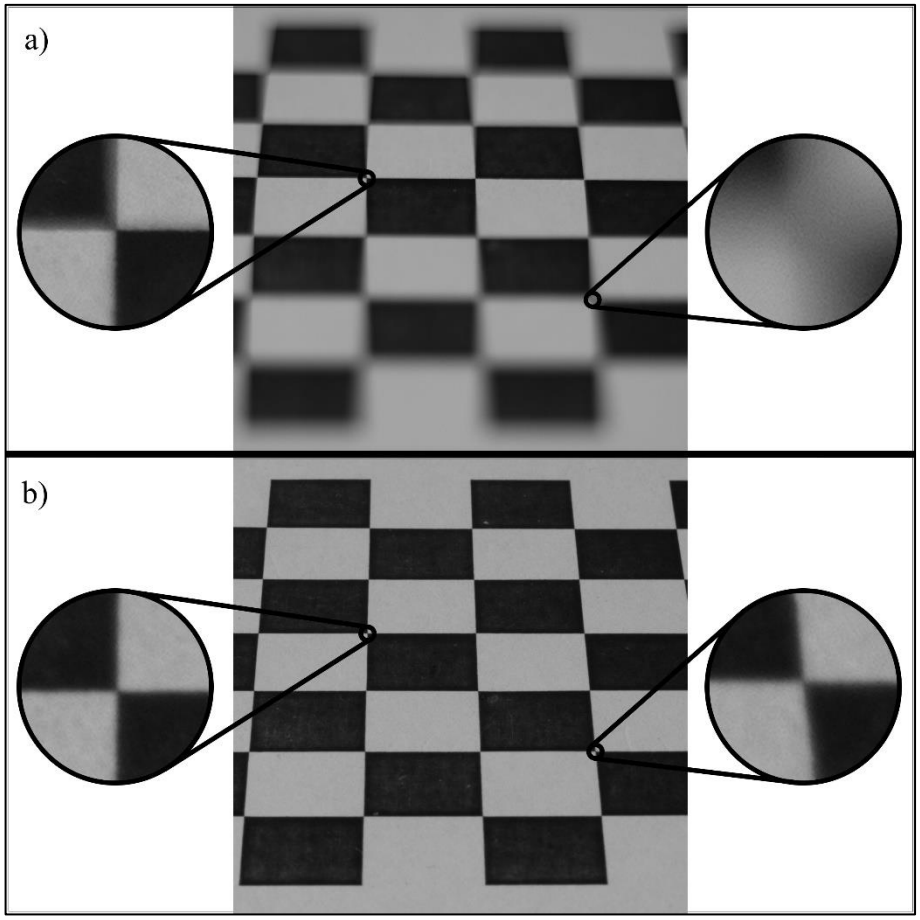

Figure 5: The Effect of Aperture on the Sharpness.

According to figure 5, in part (a) the camera aperture is set at the widest position. As can be seen the area in focus is very narrow and some part of the checkerboard is out of focus. The out of focus area causes a gaussian blur in the image which makes it harder to located the correct corner points locations in the image. On the other hand, in part (b) the aperture is adjusted to a less wide position and as the matter of the fact more area of the image is captured in focus.

All in all, higher shutter speed, lower ISO value, and closer aperture result in much sharper and cleaner frame being captured. However, to adjust all of these three settings to the desired values needs more intense light in the scene. Setting up this preparation for the camera might seem very time consuming, but nowadays consumer cameras are

adjusting these variables automatically based on the amount of light shining on the scene. Therefore, in order to have a good combination of these three factors, for the practical purposes of this set up, making sure enough light is available in the scene is important.

Resolution represents, the number of pixels the camera sensor is recording as an image inside the frame. The higher the resolution the more details can be captured on each frame. On the other hand, image compressions and noisy art effects due to encoding in the video camera can reduce the accuracy. Higher resolution needs higher data processing in the camera and to compensate, the device will compress the image more aggressively. Thus, several resolutions for the above-mentioned experiment are considered in order to find their effects on the precision and accuracy of the results.

3.3 Algorithm

The developed algorithm includes 6 steps. After recording the video of the person of interest for the posture analysis, in the first step the video as well as information regarding the checkerboard specifications video camera, namely focal length, distortion and resolution, are inserted as variables in the algorithm.

In the second step, video frames are recalled one by one for checkerboard detection. At the primary stage, in order to have more accurate measurement, built in MATLAB 'undistortImage' function is used on each frame (MATLAB, 2018b). Then after, the built in MATLAB 'detectCheckerboardPoints' function is utilized to check any checker board pattern in the frame (Geiger et al., 2012; MATLAB, 2018a). The function returns board size, rows and columns in which the corner points were detected. However, this function is design to find the best-chosen checkerboard pattern

in a frame. Therefore, when it comes to multiple checkerboards in one frame, the pixel range of corner points are masked out by setting the equivalent red, green, and blue pixel values to zero. Then after, again the "detectCheckerboardPoints" function is utilized to detect the next checkerboard. This process continues until all the expected checkerboards are detected.

The placement and order of the detected checkerboards varies from frame to frame; therefore, in the third step, the algorithm matches the checker boards. For this purpose, first, the algorithm shows the first frame with marked detected checkerboards and asks the user to specify the checkerboards one by one using color codes. Then, the algorithm calculates the pixel distances between specified checkerboards in the first frame with the ones in the next frame and arrange the checkerboards in the second frame based on closest distance of pixels. This process continues until the last frame is matched.

For the frames with less or no detection of checkerboards, the algorithm selects the previous and the next frames in which the checkerboards are detected and using linear interpolation on the coordinates of pixels in the frame, the algorithm fills out the missing corner points.

In the fourth step, the algorithm calculates the 6 DF of every checkerboard in every frame using 'extrinsics' function (Hartley & Zisserman, 2003; MATLAB, 2013; Zhang, 2000). The function returns a 3 by 3 rotation matrix as well as a 1 by 3 translation vector of the checkerboards given the image corner points, world points and camera parameters as inputs. The mathematical calculations regarding the extrinsics function are based on the PnP method.

Working with transformation matrices as the representer of 6 DF information may result in challenging conditions while rotating around the axes. One of the most common challenges is the Gimbal lock. The limitation happens when an object rotates around a certain axis by 90 degrees and loses one DF as the result of such action. In order to prevent the process from the gimbal lock complication, these transformation matrices will be converted to quaternion system using MATLAB 'rotem2quat' built-in function (Bar-Itzhack, 2000). Not only the quaternions system overcomes the gimbal lock issue, but also reduces the complexity of calculations significantly. However, it should be mentioned that in the quaternion system, location presentation is not included and the mentioned system is only capable of representing the orientation. Hence, an array of three elements is assigned for each checkerboard to track the x, y and z values representing the location separately.

In order to measure joint angles with the algorithm, relative angles are used for better presentation of orientation. For instance, as demonstrated in figure 6, in order to measure abduction, adduction, flexion and extension of the wrist joint, a marker plane is installed on the elbow above the wrist joint as the reference plane; and, another marker is placed on the posterior part of the hand as the active plane. Relative angle changes between the reference and active planes can represent the angles of abduction, adduction, flexion and extension.

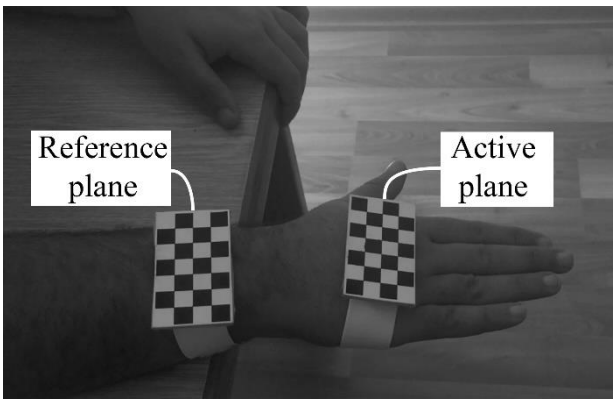

Figure 6: Active and Reference Planes for Wrist Joint Orientation

Quaternions and cartesian locations recorded in the previous step have the basis of the camera. To measure the relative orientation of the active plane, the basis should be change from the camera point of view to the reference plane. For better illustration see figure 7. For changing the basis from the camera point to the reference plane equation 7, is applied in the algorithm.

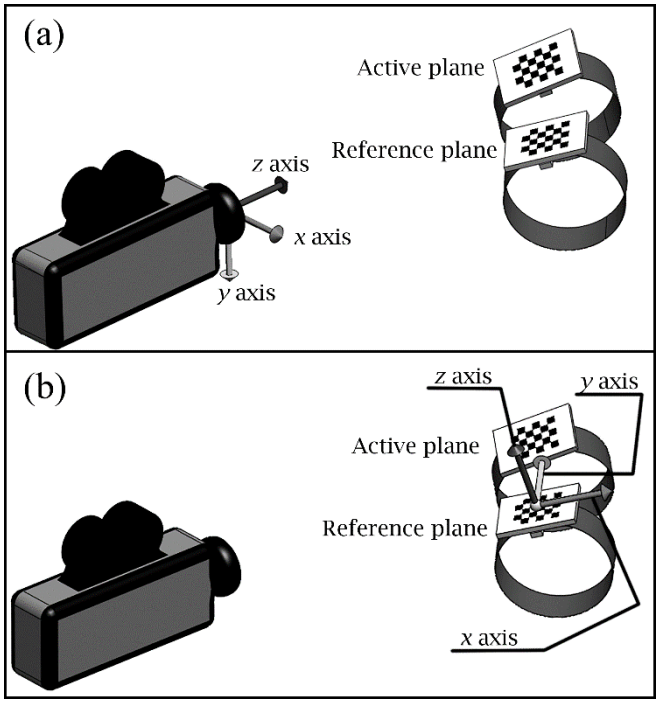

Figure 7: Change of Basis from Camera Lens (a) to Reference Plane (b)

$$Q_{new} = Q_{Reference}^{-1} \times Q_{Active} \tag{7}$$

Where Q_{new} is a one by four matrix representing quaternion numbers of the plane in the new basis. $Q_{reference}^{-1}$ is the inverse matrix of one by four matrix representing quaternion numbers of the reference plane, and Q_{Active} is the one by four matrix representing quaternion numbers of the reference plane.

In the fifth step, with the help of the user, the algorithm applies zeroing technique to compensate the offset angles of planes for further analysis. For this purpose, at the beginning of recording video the participants were asked to be in the rest position where the orientations should be considered at their zero value. The algorithm asks the user to enter the rest or default angle of joints in order to compare them with the first frame of the video. In case of any offset from the entered value, the algorithm considers the difference as an offset value and adjust the rest of the measurements accordingly.

In the last step, since reading quaternion values are difficult, the algorithm converts these values to Euclidean angles and cartesian coordinates. Moreover, for demonstration of the process, a subplot is provided where the orientation values are illustrated as a line chart as well as the recorded video with detected checkerboards and a 3D simulated space of the movement. For better understanding of the algorithm a detailed flow chart is provided in Appendix A. Moreover, the following is pseudocode of the developed algorithm:

1. Begin
2. Input camera calibration parameters as variable cam
3. Input the video file as variable vid
4. Save the total number of video frames from vid as variable n
5. Input the total number of checkerboards in each frame as variable numOfCB

6. Save the world points 3D coordinates from the cam into variable wP

7. Input the number of rows and columns to be detected in variable bSize

8. Set i = 1 as the loop counter

9. Initialize cell variable bPs

10. While i <= n, repeat steps 10 to 22

11. Save frame i from vid as variable f

12. Make frame undistorted using cam and save into variable im

13. Set j = 1

14. If j > numOfCB go to step 22

15. Save the pixel point values from detected checkerboards of im into variable imP

16. If imP = bSize, then go to step 16, elseif imP = 0, then set bPs(i, j) to Nan (Not a number) and go to step 22, else go to step 19

17. Append imP into bPs(i, j)

18. Save inner points in variable bP

19. Set pixel values of im image to zero within the range of bPs

20. j = j+1

21. Go to step 14

22. i = i+1

23. Save frame 1 in f

24. Put markers on f according to bPs(1, from 1 to numOfCB) pixel locations

25. Display f and the markers

26. i = 1

27. Initialize cell variable name

28. If i > numOfCB, then go to step 34, else,

29. Output “Name checkerboard I”

30. Input the user respond into name(i, 1)
31. Output “Click on the” + name(i, 1) + “checkerboard”
32. Input the mouse click x, and y coordinates intro name(i, from 2 to 3)
33. i = i+1 and go to step 28
34. Calculate the centroid of the image points for each checkerboard in each frame
35. Set i = 2
36. If i > n, then go to step 40
37. Calculate Euclidian distances between each checkerboard location at frame i and frame i -1 and save the values in oBPs
38. Reorder checkerboards based on the minimum calculated distances in oBPS
39. i = i+1 and go to step 36
40. set i = 1
41. If i > n, then go to step 47
42. Set j = 1
43. If j > numOfCB, then i = i+1 and go to step 41
44. Save rotation and translation matrices from oBPs(i, j) into rotM and trM variables using wP, cam variables and extrinsics built-in function
45. Save the quaternion transform of rotMat into cell variable Quats(i, j)
46. j = j+1 and go to step 43
47. Change the basis from center of the camera to the reference checkerboard
48. Create multi-layer output variable matrix of n by 6 by numOfCB
49. Transform quaternion values to x, y, and z Euler angles and save as variable Angles
50. Set variable dif as [0, 0, 0] – trM of reference checkerboard
51. Save trM+dif into variable newTrMs

52. Append newTrMs in outPut multi-layer matrix variable columns 1 to 3 and append relevant Euler angels in columns 4 to 6, each layer of the matrix variable representing a checkerboard
53. Output as Comma Separated Values (.csv)
54. Export a video with 3D simulation of checkerboards, the video it self and x y z line chart in a subplot environment
55. End

3.4 Reliability Test Experiment

To analyze the precision of the algorithm measurements many dependent and independent factors are involved. Therefore, in this study an experiment is designed to analyze the algorithm performance.

This experiment investigates the effect of combination of corner points with different square sizes of the checkerboards and video resolution, on the precision of 3D locations and orientations. The experiment has three independent factors and two dependent factors. Table 1 demonstrates types of independent variables with their levels of treatments. In order to select the potential combination of the corner points for the experiment, the size limitation of the markers has been considered to be less than or equal to 6×7 cm in order for the markers to be usable for smaller body parts such as forehead or posterior part of the hand for posture tracking. Moreover, the combinations were considered as odd number in one direction and even number on the second direction in order to keep the markers asymmetry as explained in section 2.1. Furthermore, the selected frame resolutions were based on the current smart phone camera capabilities in order to avoid involving professional camera equipment as a necessity for utilizing this algorithm. It should be mentioned that the aspect ratios of

selected resolution are set to 4×3 rather than 16×9 in order to capture more information on each frame and have a wider angle of view.

Table 1: Representation of Experiment

Variable	Type	Treatment level
Corner points	Categorical	Pattern: 3×4, Square side size of: 8 (mm)
		Pattern: 4×5, Square side size of: 8 (mm)
		Pattern: 5×6, Square side size of: 8 (mm)
		Pattern: 3×4, Square side size of: 10 (mm)
		Pattern: 4×5, Square side size of: 10 (mm)
		Pattern: 5×6, Square side size of: 10 (mm)
		Pattern: 3×4, Square side size of: 12 (mm)
		Pattern: 4×5, Square side size of: 12 (mm)
Resolution (Pixels)	Categorical	1920×1440
		2560×1920
		3200×2400
		4000×3000
Axes	Categorical	x axis
		y axis
		z axis

To run the experiment, a 60×60 cm^2 platform is designed to contain 25 checkerboards in different locations and orientations. This platform is located in front of a camera at the distance of 110 cm and the video is recorded at 24 frames per seconds for every combination of independent variables. Videos are recorded for 4 to 5 seconds in every test run in order to collect approximately 100 measurements of 6 DF for each checkerboard. It should be mentioned that, each video frame is one instance of measurement for 6 DF of each checkerboard. The videos are recorded indoor, placed close to windows to utilize enough exposure from sunlight. In order to minimize the error due to camera shakes, the camera is installed on a tripod and remotely controlled for collecting videos. The recorded videos are analyzed by the algorithm and respective data regarding orientations and locations of the checkerboards are gathered.

Figure 8 illustrates the design of the platform. The checkerboards are marked from A1 to E5. Table 2 represents the 6 DF true values measured by ruler and protractor.

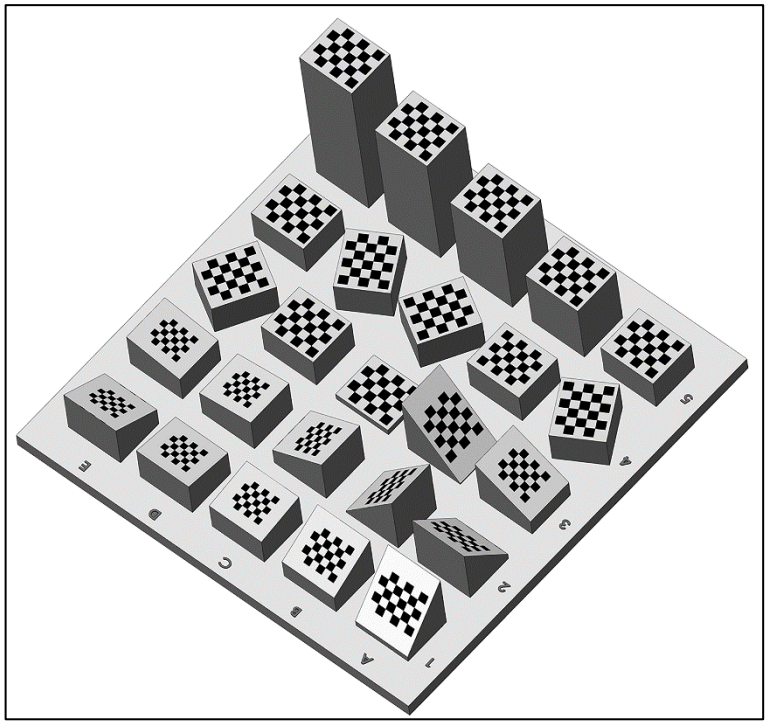

Figure 8: Designed Platform for the Experiment

For testing the precision of the measurement as the dependent variable, the Standard Deviations (SDs) of approximately 100 data points of 6 DF of each checkerboard in each video are calculated. The measurements during the 4 to 5 second video recording are supposed to be constant given the fact that in every video, both camera and the checkerboards are at the same position during the recording. Therefore, in order to find the measurement variations from the true value, the SDs of the mentioned 100 data points of 3D locations and orientations, are selected as the factor showing the precision of the algorithm measurements.

Table 2: Relative Orientation and Location of Each Checkerboard

Plane	*x* (mm)	*y* (mm)	*z* (mm)	*x*°	*y*°	*z*°
A1	-220	220	76	0	50	0
B1	-110	220	76	0	30	0
C1	0	220	76	0	10	0
D1	110	220	76	0	-10	0
E1	220	220	76	0	-30	0
A2	-220	110	76	0	-50	0
B2	-110	110	76	50	0	0
C2	0	110	76	30	0	0
D2	110	110	76	-10	0	0
E2	220	110	76	10	0	0
A3	-220	0	0	0	0	60
B3	-110	0	0	0	0	0
C3 (Reference)	**0**	**0**	**0**	**0**	**0**	**0**
D3	110	0	76	-50	0	0
E3	220	0	76	-30	0	0
A4	-220	-110	0	0	0	360
B4	-110	-110	0	0	0	300
C4	0	-110	0	0	0	240
D4	110	-110	0	0	0	180
E4	220	-110	0	0	0	120
A5	-220	-220	110	0	0	0
B5	-110	-220	160	0	0	0
C5	0	-220	210	0	0	0
D5	110	-220	260	0	0	0
E5	220	-220	310	0	0	0

Regarding the statistical test, the distributions of the dependent variables are analyzed and accordingly, Kruskal-Wallis statistical tests applied. It should be mentioned that even though the measurement were done on the same platform after each video at least one of the treatment levels of the independent factors namely resolution of the video or pattern of the checkerboards which are mentioned Table 1 is changed in order to make the measurements data independent from each other. The following hypotheses are assumed for the statistical analyses.

- H1: The corner points pattern of checkerboards significantly affects the precision of orientation measurement.
- H2: The corner points pattern of checkerboards significantly affects the precision of location measurement.
- H3: The video resolution significantly affects the precision of orientation measurement.

- H4: The video resolution significantly affects the precision of location measurement.
- H5: The axes significantly affect the precision of orientation measurements.
- H6: The axes significantly affect the precision of location measurements.

Related to the first 2 hypotheses, the corner points pattern of checkerboards is considered as the number of rows and columns of inner points of the checkerboard and the distance of the points from each other in the video frame as mentioned in Table 1. It is hypothesized that the greater the number of inner points and the further the distance of them from each other provides a more precise 3D representation of checkerboard locations and orientations. Moreover, related with the third and fourth hypotheses, it is anticipated that higher resolution of video could results in a more precise location of the detected inner points and consequently more precise results for 3D representation. Regarding the last two hypotheses, it is conjectured that the measurement precision might differ in z axis as shown in figure 7. To be more specific, since the *z* axis represents the location depth of a 2D image, lower precision is expected compare to *x* and y axes. On the other hand, since rotation around *z* axis can have the range of 360 degrees as demonstrated in figure 2, it is anticipated that the rotation around this axis will be more precise than x and y.

3.5 Validation of the Algorithm

To validate the utilization of the algorithm for the purpose of real-life posture analysis, an experiment is selected based on the study conducted by Roby-Brami et al. (2020). In their study, they used EMT device to compare head and trunk orientation during pointing and looking at an object. For this purpose, they provided 8 evenly distributed targets along the circumference of a circle with the radius of 32 cm. Targets were

placed at 95 cm distance from 10 participants. Then participants were asked to both point at and look at each of the targets in 3 blocks of nine movements, in random orders. Thus, 27 movement of pointing and 27 movements of looking was recorded from each participant using four electromagnetic sensors.

In order to conduct the same experiment for the purpose of validation, similar target board was created. Ten participants aged between 29 and 38 volunteered to partake in the experiment similar to the mentioned study. One checkerboard was attached to the forehead, one attached to the skin over the manubrium and one was attached separately on a surface in front of the participant as the reference board.

The ethical approval was granted to the study by Ethic Board of Engineering at Eastern Mediterranean University for the protection of the individuals participating in the experiment (Ref. No. ETK00-2021-0063 date 26.03.2021). All participants provided informed consent form prior to the experiment.

A camera was fixed on a tripod in front of the participants and align to put all the three checkerboard markers in the frame. Since the reference study set the frequency of data gathering at 30 Hz, in this study the camera was set to 30 frames per second. Prior to the experiment, camera was calibrated using one of the checkerboard markers according to section 2.2.

After attaching the checkerboard markers, participants were asked to algin their feet, at the malleoli, to a marked line 95 cm away from the target board. Then, based on the height of each individual, the height of the target board was adjusted in order to keep the center of target board in the line of sight at upright standing position. In order to

keep the content within the scope of the study and fulfill the objective of the experiment, in this study only looking at the target was included in the experiment. Therefore, while recording with the camera, the participants were asked to look at the center at the beginning of the experiment and after the completion of each block for the purpose of zeroing. Participants, looked at 9 random targets, instructed by the experimenter, and repeat the task for three blocks in total, similar to the reference study.

In order to measure the head orientation along the three axes, after zeroing and aligning the axes of chest and head checkerboards to the reference board, basis was changed from the center of the camera lens to the checkerboard attached to the chest using equation 1. Relative head checkerboard orientations along x, y and z axes were assigned to Anteroposterior tilt, Axial rotation and Lateral tilt, respectively. In order to compare the data gathered from this study with the reference study, average difference of x, y and z angles, recorded by the developed algorithm and the data presented in the study was calculated. Additionally, one sample T-test was used to check whether there is a significant difference between the data recorded by the developed algorithm and the data recorded in the reference study.

Chapter 4

RESULTS

After developing the algorithm, in order to test it, two checkerboards are installed according to the fourth step in the methodology section. A video was recorded while a participant applied flexion, extension, abduction and adduction on his wrist. Relative angles were calculated using the algorithm and a synchronized version of the action (top right), 3D simulated spaces (Top Left) and joint relative angles (Bottom) was exported and is shown in the exported video provided in figure 9.

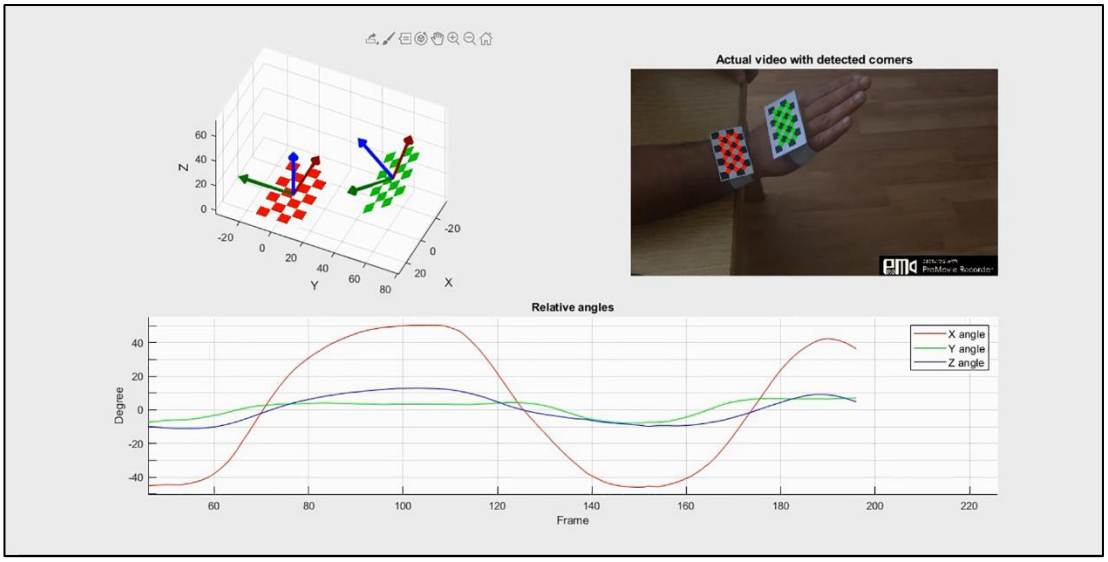

Figure 9: Algorithm Results for Measuring Wrist Angle Joints

The video taken from the action is shown in the figure 9, at the top right section. Detected corner points which are marked with green color demonstrates the active plane and detected corner points were marked with red color represent the reference plane. In the top left section, a 3D environment related to the movements of the planes

simulated. The green checkerboard represents the active plane and the red checkerboard represents the reference plane. In the bottom section of the figure, Euclidian angles measured between to checker boards which represent the angles of the wrist joint are illustrated as a line graph. In the mentioned graph, red line shows the angle of x axis on the basis of the reference plane which is equivalent angle of wrist extension if the x value is positive or wrist flexion if the x value is negative. Similarly, the blue color shows the angle of z axis on the basis of the reference plane which is equivalent angle of wrist adduction if z value is positive or wrist abduction if the z value is negative. Likewise, the green color represents the pronation and supination angles. It should be mentioned that considering the checkerboard set up of the figure the algorithm is incapable of measuring any pronation or supination in the wrist joint as such actions is generated from Ulna and Radius bones in the lower arm region. In order to measure any pronation or supination, another checkerboard needs to be installed above the elbow for the necessary measurements. Finally, at the time instance which the frame of figure 4 is captured, the participant is returning to the rest position from an extension action on the rest and in the line chart, the graph shows a close to 40-degree angle for the x value.

Regarding the performance analysis, 32 videos were taken from each combination of resolutions and corner points pattern. According to table 1 in the Methodology chapter there are 8 corner point patterns and 4 video resolution. At every run of the experiment the checkerboards of one corner point pattern were attached to the platform and for each of the patterns 4 videos were taken each at different resolution. Thus, totally 32 videos were taken from each combination of the mentioned independent factors. The duration of each video was between 4 and 5 seconds at 25 FPS. Both camera and the

checkerboards were fixed at the distance of 1 meter apart from each other. The difference between measured orientation and location of the checkerboards and the expected distances from table 2 was calculated. Then to find the precision of the algorithm, SD of each checkerboard was calculated for 6 DoF in each video.

Three independent variables with eight, four and three different levels of treatments plus 24 measurements (25 checkerboards as shown in figure 8 minus checker board C3 which was considered as the reference and basis) of each combination as replications gave us 4800 data for statistical analyses. For the necessary statistical analyses, this study used the SPSS software of version 22.0. In order to investigate the distribution of the mentioned data, the histogram of the data (see figure 10) as well as Q-Q plots (see figure 11) are illustrated for location precision in mm. Moreover, figure 12 and 13 present the histogram and Q-Q plot of the orientation precision in degrees, respectively.

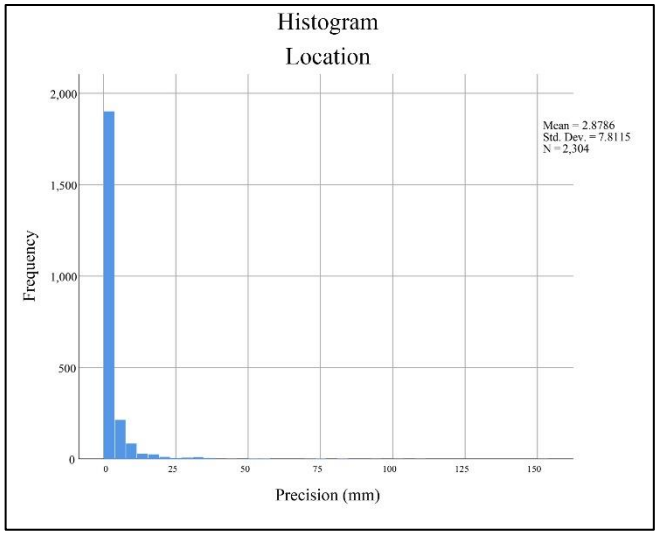

Figure 10: Histogram of Location Precision Distribution

According to the histogram provided in figure 10, the distribution of the location data is highly skewed to the right while the frequency of the data picking at a value close to zero. This is due to the fact that the SD of each measurement was considered as the precision value which cannot result in any negative value.

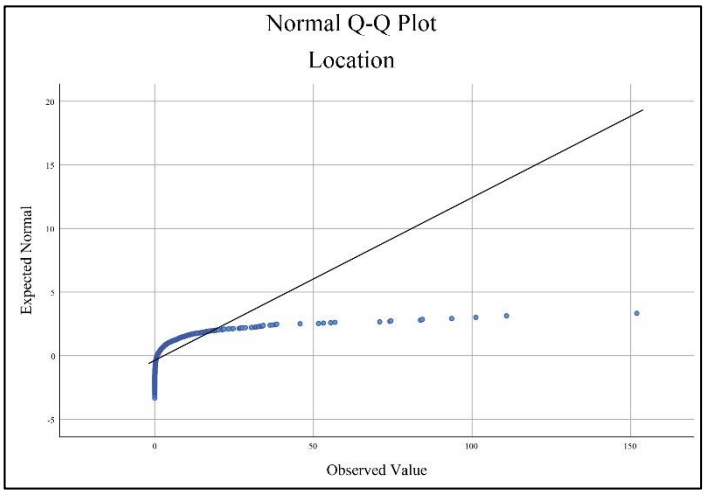

Figure 11: Normal Q-Q Plot for Location Precision Distribution

In figure 11, normal Q-Q plot of the same data is presented. This figure is provided to present the values at extreme in a clearer illustration as well as investigating the possibility of the data presenting a logarithmic normal distribution. According to this figure, a significant divergence of the data is observable in comparison with an expected 45° reference normal line.

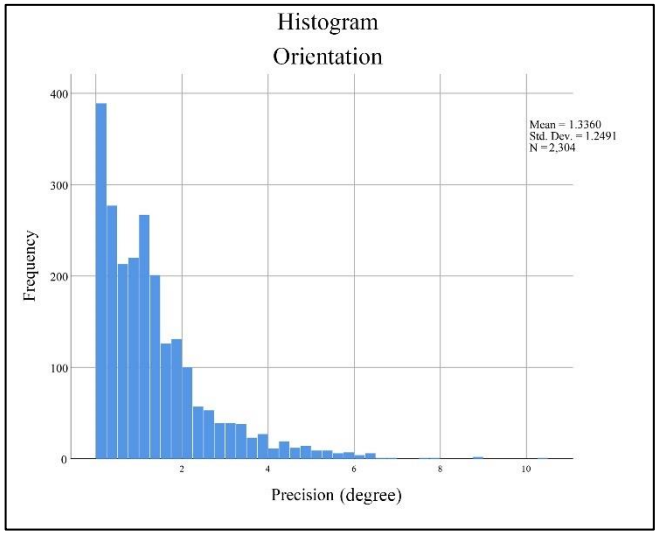

Figure 12: Histogram of Orientation Precision Distribution

Figure 12 present the distribution of the SD of the orientation measurement from the true value. Similar to Figure 10, the distribution is highly skewed to the right with the a few extreme values beyond 10° on the right side.

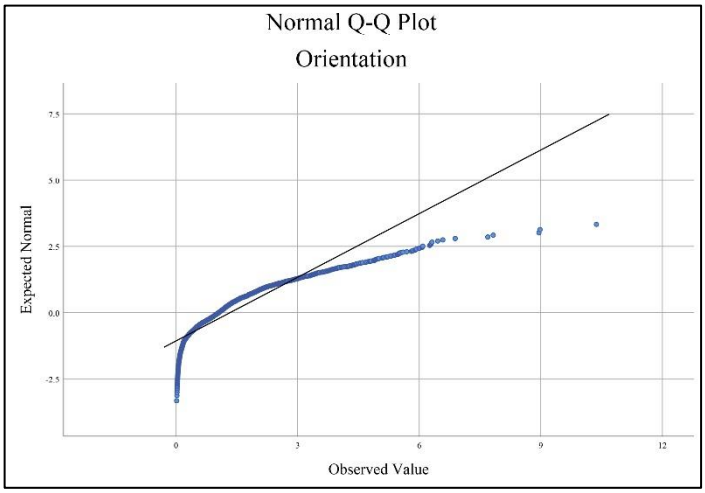

Figure 13: Normal Q-Q Plot for Orientation Precision Distribution

Because, the extreme values are not presented clearly on figure 12, figure 13 is provided. The figure presents the normal Q-Q plot of the calculated orientation SDs. Similar to figure 11, the measured data is not following the 45° reference line.

As mentioned, the gathered data is describing precision and it is highly skewed to the right, a log normal distribution pattern is been expected. Therefore, the logarithmic values of the data were calculated and once more histograms and normal Q-Q plots are illustrated (see figures 14 to 17).

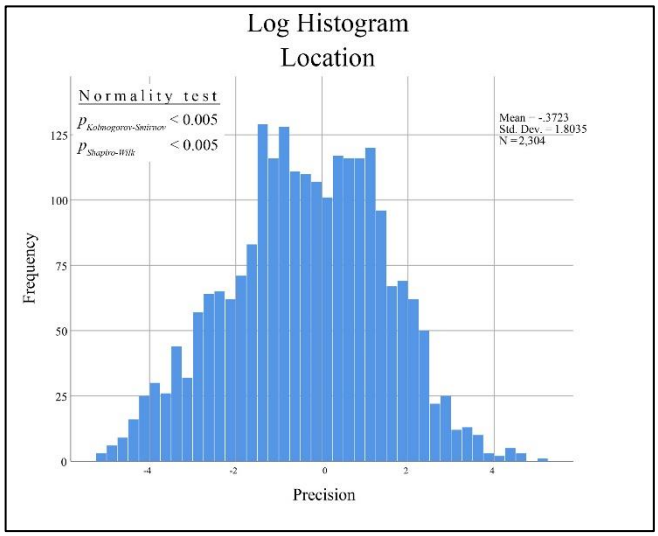

Figure 14: Log Histogram of Location Precision Distribution

Figure 14 presents the logarithmic values provided in figure 10. The base of the logarithm is set to the Euler's number (e ≈ 2.718). Accordingly, this modification provides a histogram which closely follows the normal distribution. However, further statistical tests are provided later on this chapter which shows a significant difference between the normal distribution and the lognormal values.

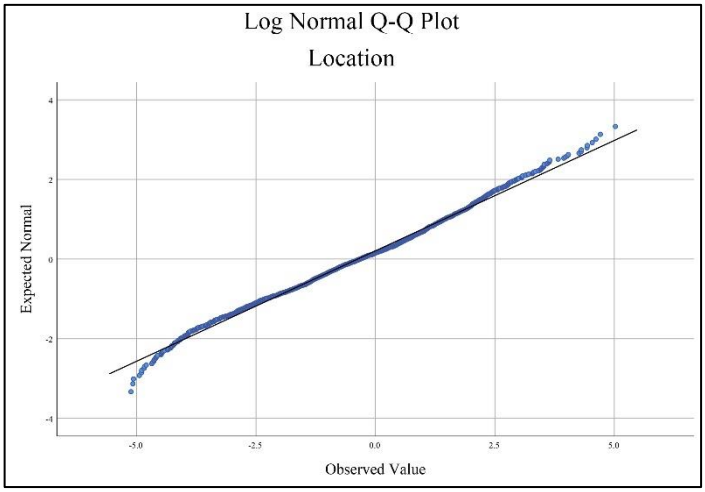

Figure 15: Log Normal Q-Q Plot for Location Precision Distribution

In figure 15, the normal Q-Q plot of the ln of the location data is illustrated. According to the figure, the data lies closely on the 45° reference line with less values at extreme.

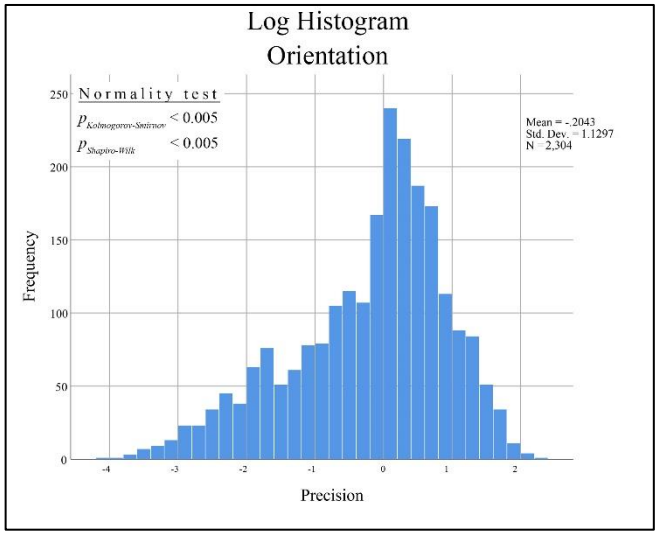

Figure 16: Log Histogram of Orientation Precision Distribution

Similar to figure 14, figure 16 demonstrates the natural log of the orientation data. This modification brings the distribution curve closer to a normal distribution. However, in comparison with location data a left skew is observable in the histogram.

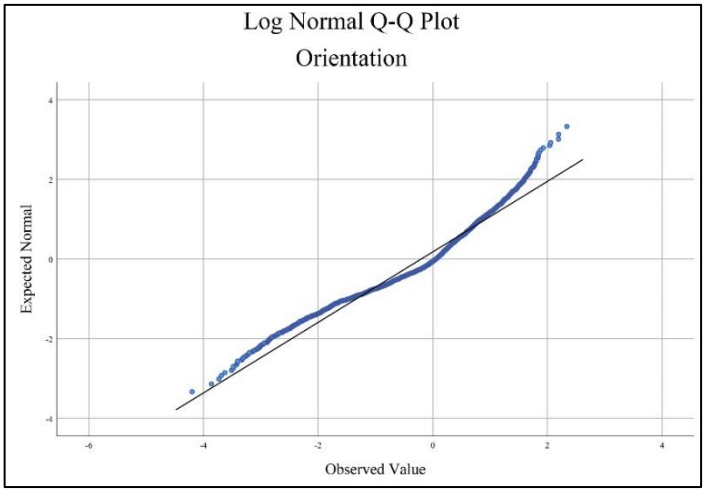

Figure 17: Log Normal Q-Q Plot for Orientation Precision Distribution

Figure 17, represents the normal Q-Q plot of the ln of orientation data. Less values at extreme are observable in this figure. However, the data values do not completely lie on the 45° reference line and the end tail of the data at the top right of the figure show a divergence towards left.

Even though the distribution patterns got closer to normal distribution, the Kolmogorov-Smirnov and Shapiro-Wilk tests of normality both had the $p < 0.005$ with test statistics 0.036 (location), 0.102 (orientation) and 0.0995 (location), 0.0690 (orientation), respectively. Thus, for statistical analyses, non-parametric independent-samples Kruskal-Wallis test was applied (see table 3). It should be mentioned that the selected test is incapable of measuring significant intersection between factors. However detailed pair comparison of each level is provided in tables 4, 5, and 6 for corner point pattern, resolution, and axes factors respectively. Furthermore, for demonstrating the significant effect of each level of treatment, box plot of corner point pattern, resolution, and axes factors are provided on figures 18, 19, and 20, respectively.

Table 3: Independent-Samples Kruskal-Wallis Test Result

Hypothesis	Test *p*	Independent factor	Dependent factor
H1	<0.001	Corner points pattern	Orientation precision
H2	<0.001	Corner points pattern	Location precision
H3	0.005	Video Resolution	Orientation precision
H4	0.112	Video Resolution	Location precision
H5	<0.001	Axes	Orientation precision
H6	<0.001	Axes	Location precision

According to table 3, and considering the type I error of 0.01 percent, except H4 which tests the significant effect of video resolution on the location precision, all other independent factors significantly affect the precision of both location and orientation.

Table 4: Pair Comparison Test for Corner Pattern

Comparison	Location		Orientation	
	Test statistic	p-value	Test statistic	p-value
3×4-08mm vs 3×4-10mm	68.16	0.209	204.44	>0.001
3×4-08mm vs 3×4-12mm	315.46	>0.001	641.13	>0.001
3×4-08mm vs 4×5-08mm	252.4	>0.001	303.53	>0.001
3×4-08mm vs 4×5-10mm	341.9	>0.001	691.78	>0.001
3×4-08mm vs 4×5-12mm	442.98	>0.001	817.96	>0.001
3×4-08mm vs 5×6-08mm	300.85	>0.001	654.13	>0.001
3×4-08mm vs 5×6-10mm	680	>0.001	1180.25	>0.001
3×4-10mm vs 3×4-12mm	247.3	>0.001	436.69	>0.001
3×4-10mm vs 4×5-08mm	184.24	0.001	99.09	0.068
3×4-10mm vs 4×5-10mm	273.74	>0.001	487.33	>0.001
3×4-10mm vs 4×5-12mm	374.81	>0.001	613.51	>0.001
3×4-10mm vs 5×6-08mm	232.69	>0.001	449.69	>0.001
3×4-10mm vs 5×6-10mm	611.84	>0.001	975.8	>0.001
3×4-12mm vs 4×5-08mm	-63.05	0.245	337.6	>0.001
3×4-12mm vs 4×5-10mm	26.44	0.626	50.65	>0.001
3×4-12mm vs 4×5-12mm	127.52	0.019	176.83	0.001
3×4-12mm vs 5×6-08mm	-14.61	0.788	539.12	>0.001
3×4-12mm vs 5×6-10mm	364.55	>0.001	539.12	>0.001
4×5-08mm vs 4×5-10mm	89.5	0.099	388.25	>0.001
4×5-08mm vs 4×5-12mm	190.57	>0.001	514.42	>0.001
4×5-08mm vs 5×6-08mm	48.44	0.372	350.6	>0.001
4×5-08mm vs 5×6-10mm	427.6	>0.001	876.71	>0.001
4×5-10mm vs 4×5-12mm	101.08	0.063	126.18	0.02
4×5-10mm vs 5×6-08mm	-41.05	0.449	37.65	0.488
4×5-10mm vs 5×6-10mm	338.11	>0.001	488.47	>0.001
4×5-12mm vs 5×6-08mm	-142.13	0.009	163.83	0.003
4×5-12mm vs 5×6-10mm	237.03	>0.001	362.29	>0.001
5×6-08mm vs 5×6-10mm	379.16	>0.001	526.12	>0.001

Table 4, presents the pair comparison of different levels of corner point patterns. Accordingly, the p values less than 0.01 points out that there is a significant difference between the selected two levels. Negative values of the test statistic column in this

table demonstrate higher precision of the left primary level in comparison with the secondary level (referring to the first column of the table).

Table 5: Pair Comparison for Resolution

Comparison	Orientation	
	Test statistic	p-value
1920×1440 vs 2560×1920	45.71	0.234
1920×1440 vs 3200×2400	47.39	0.217
1920×1440 vs 4000×3000	68.86	0.073
2560×1920 vs 3200×2400	1.67	0.965
2560×1920 vs 4000×3000	114.58	0.003
3200×2400 vs 4000×3000	116.25	0.002

Same as table 4, table 5 shows the pair comparison result of the resolution factor for orientation. No pair comparison is provided for location in this table since there is no significant difference between the levels. However, in location significant differences are shown for 2560×1920, and 3200×2400 resolutions, in comparison with 4000×3000 resolution. Given the fact that the negative values were observed in the test statistic column for the mentioned levels, less precise orientation data are measured with 4000×3000 resolution.

Table 6: Pair Comparison for Axes

Comparison	Location		Orientation	
	Test statistic	p-value	Test statistic	p-value
x vs y	67.51	0.042	154.23	>0.001
x vs z	932.41	>0.001	1011.52	>0.001
y vs z	864.90	>0.001	857.29	>0.001

Lastly, table 6 shows the pair comparison result of the axes factor on both locations and orientations. According to this figure, z-axis significantly effects the precision of both location and orientation measurements. For location measurement, the positive values present a more precise measurement when comparing x-axis and y-axis to the z axis while opposite results are presented regarding the orientation measurement.

Additionally, significantly more precise orientation measurement is achieved on the x-axis in comparison with the y-axis.

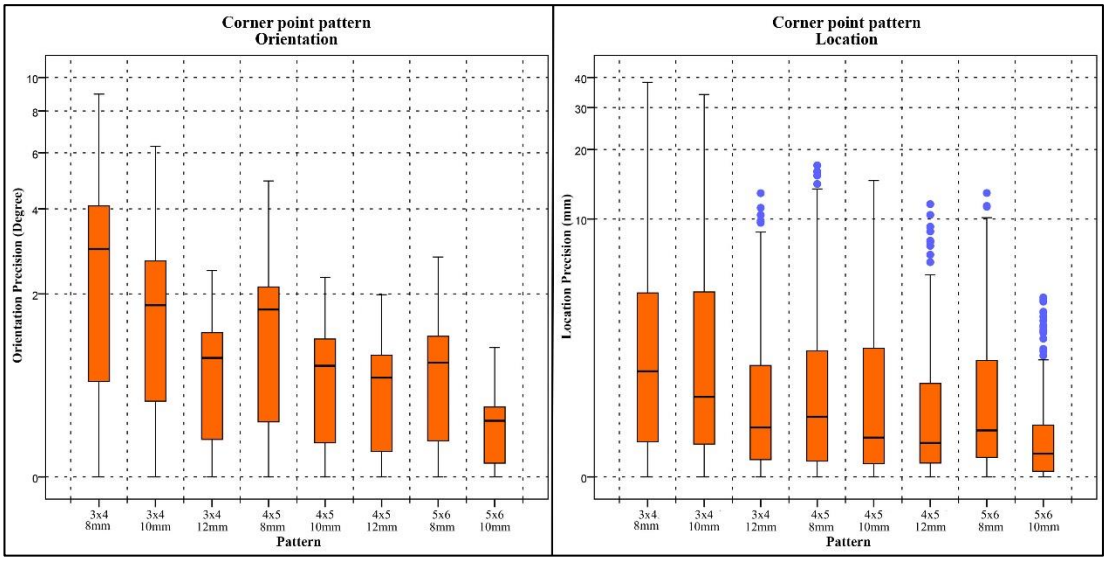

Figure 18: Box Plot of Corner Point Pattern Factor

In order to provide a better representation of the difference in corner point patterns, both location and orientation box plots are provided in figure 18 for each pattern. Based on the figure, the more rows and columns in the pattern and the bigger the size of the squares the more precise measurement is achieved. It should be mentioned that the vertical axes units are increased logarithmic rather than linearly in order to provide a more readable figure.

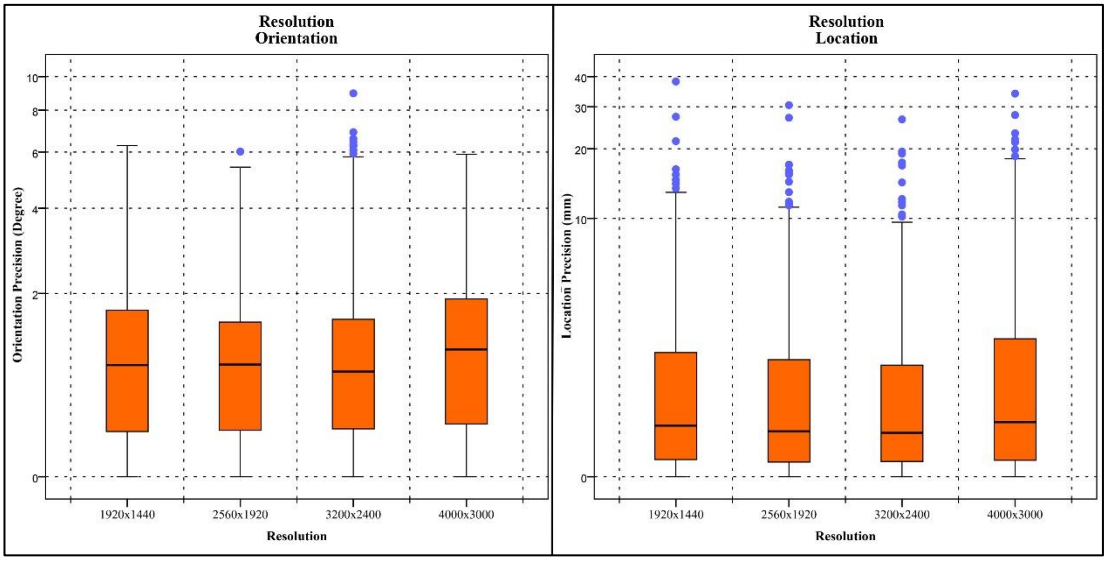

Figure 19: Box Plot of Resolution Factor

Figure 19, demonstrates the spread of data precision in different resolution level. Based on the figure as well as table 3, location precision does not significantly differ along different levels. However, significantly less precise measurement is observed on the orientation plot. Similar to figure 18 the horizontal axis follows a logarithmic distribution for better data presentation.

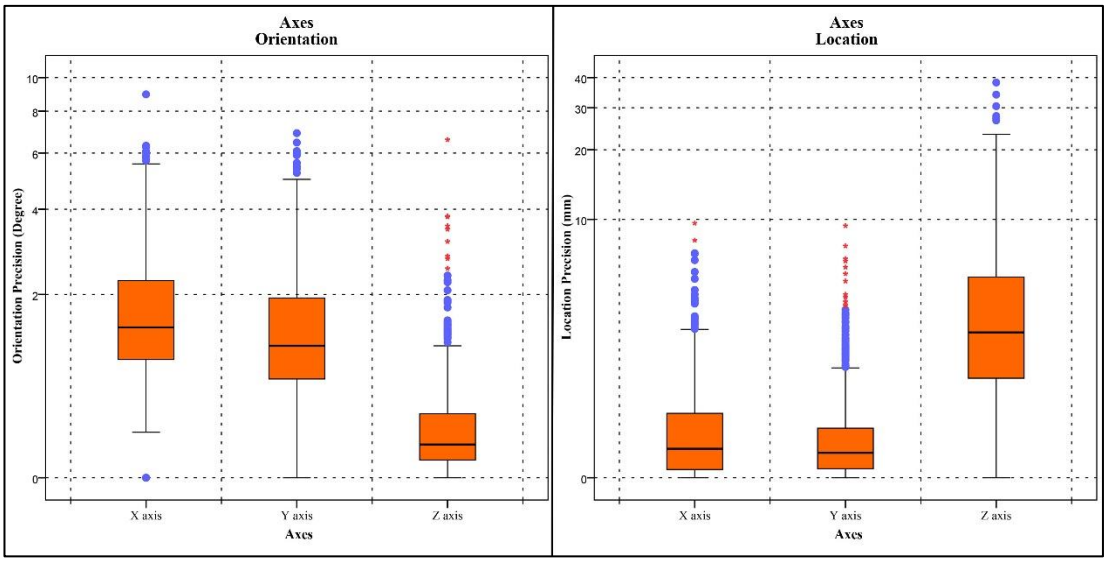

Figure 20: Box Plot of Axes Factor

Lastly, box plot of location and orientation precision along different axes of the reference plane is provided in figure 20. Even though, more precise measurement was achieved along x and y axes compared to the z axes locations, contradictory results are shown for orientation precision.

In order to measure the power of the test Operating Characteristic (OC) curve method was used. Given the fact that no intersection was statistically assessed, each of the three factors were considered as a single factor factorial experiment design. Accordingly, table 7 shows the related test power of each factor. It should be mentioned that for the calculation of the power, overall mean of the location and orientation precisions are 1.263mm, and -0.78044°, respectively. Moreover, overall variances of location and orientation precisions are 385.359 and 27.095, respectively.

Apart from the none parametric statistical test, error of the data was calculated from the true values of the platform. In comparison with the precision data, the distribution of calculated error data is much closer to a normal distribution.

In order to demonstrate the distribution of error values, the histograms of the data are illustrated in the appendices section. Thus, Appendix B, and C illustrate the histograms of error data based on different corner point patterns for location, and orientation, respectively. Furthermore, Appendix D shows the histogram data based on the resolutions factor. The left side shows the distribution of location error in mm and the right side shows the distribution of orientation error in degrees. Similarly, the Histograms of axes are provided in Appendix E.

Table 7: Test Power of the Factors

Factor	Level	mean	n	Φ^2	Φ	a(n-1)	β	Power
Corner point pattern								
For location	4x5-08mm	-0.74	264	12.84	3.58	2104	<1%	>99%
	4x5-10mm	1.05	261	12.70	3.56	2080	<1%	>99%
	4x5-12mm	0.98	270	13.14	3.62	2152	<1%	>99%
	5x6-08mm	-0.36	267	12.99	3.60	2128	<1%	>99%
	5x6-10mm	11.79	282	13.72	3.70	2248	<1%	>99%
	5x6-12mm	-2.75	276	13.43	3.66	2200	<1%	>99%
	6x7-08mm	-2.56	282	13.72	3.70	2248	<1%	>99%
	6x7-10mm	2.40	273	13.28	3.64	2176	<1%	>99%
For orientation	4x5-08mm	-2.15	264	20.03	4.48	2104	<1%	>99%
	4x5-10mm	-2.07	261	19.80	4.45	2080	<1%	>99%
	4x5-12mm	-1.79	270	20.48	4.53	2152	<1%	>99%
	5x6-08mm	-1.07	267	20.26	4.50	2128	<1%	>99%
	5x6-10mm	2.31	282	21.40	4.63	2248	<1%	>99%
	5x6-12mm	-0.36	276	20.94	4.58	2200	<1%	>99%
	6x7-08mm	-1.66	282	21.40	4.63	2248	<1%	>99%
	6x7-10mm	0.35	273	20.71	4.55	2176	<1%	>99%
Resolution								
For location	1920x1440	1.04	531	0.05	0.23	2123	>99%	<1%
	2560x1920	0.97	549	0.05	0.23	2195	>99%	<1%
	3200x2400	1.37	546	0.05	0.23	2183	>99%	<1%
	4000x3000	1.66	549	0.05	0.23	2195	>99%	<1%
For orientation	1920x1440	-0.93	531	0.11	0.34	2123	>99%	<1%
	2560x1920	-0.70	549	0.12	0.34	2195	>99%	<1%
	3200x2400	-0.66	546	0.12	0.34	2183	>99%	<1%
	4000x3000	-0.83	549	0.12	0.34	2195	>99%	<1%
Axes								
For location	X	-2.80	725	7.82	2.80	2172	3%	97%
	Y	1.24	725	7.82	2.80	2172	3%	97%
	Z	5.35	725	7.82	2.80	2172	3%	97%
For Orientation	X	-0.83	725	12.79	3.58	2172	<1%	>99%
	Y	-2.14	725	12.79	3.58	2172	<1%	>99%
	Z	0.63	725	12.79	3.58	2172	<1%	>99%

According to table 7, the power of the tests was calculated. Except the resolution factor, above 95% of power was observed for each factor. The necessary equations for the calculation of test power is provided in the book of Montgomery (2017). It should be mentioned that the power estimation requires the normality assumption to be held. However, due to the highly skewed distribution of the sample data the achieved power tests are not significantly reliable and needs further investigation.

Regarding the validation experiment, all the data was analyzed with the developed algorithm. Head orientations were collected for each target from the frame which head reached the maximum rotation and stopped at target, to the frame which the head starts

moving towards the next target point. The average of *x, y* and *z* values were calculated in order to record the amount of Anteroposterior tilt, Axial rotation and Lateral tilt of each target in degrees. Figure 10 demonstrates the average data measured with the developed algorithm compare to the data measured with EMT device in the reference study. Finally, mean and SD of all the recorded targets was recorded and presented in Table 4, followed by the values presented in the reference study conducted by Roby-Brami et al. (2020). Furthermore, in order to use one sample T-test for statistical analysis, the differences of mean values are provided on Table 4.

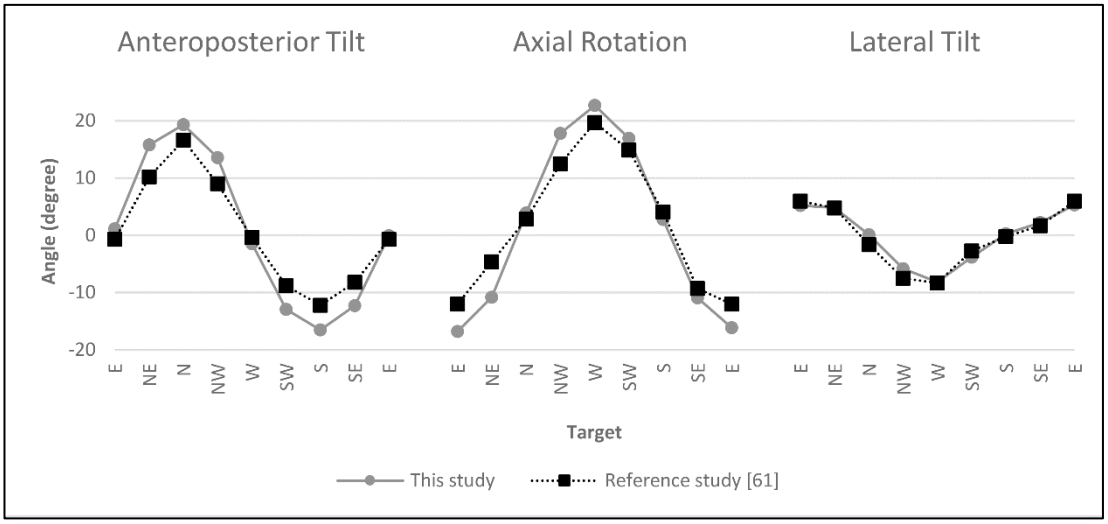

Figure 21: Comparison between this Algorithm and the Reference Study

Figure 21, demonstrate the comparison between the orientation measurement of the neck relative to chest collected using algorithm and the reference study (Roby-Brami et al., 2020). Even though very close measurements are observable in all orientation axes, slight divergence is observable in A/P tilt, and AR when it gets close to 20° of rotation. It should be mentioned that E, N, NE, NW, S, SE, SW, and W stand for East, North, North East, North West, South, South East, South West, and West directions, respectively. Furthermore, detailed values of mean and SD as well as the difference

between the measurement of the algorithm and the reference study is provided in Table 4. The direction abbreviations in the table follow the same rule as figure 21.

Table 8: Relative Head Orientation Compare to the Reference Study

Method			E	NE	N	NW	W	SE	S	SW
This study	A/P tilt	Mean	1.1	15.8	19.3	13.6	-1.5	-12.9	-16.5	-12.3
		SD	1.4	4.7	5.7	4.5	2.4	2.2	2.1	2.5
	AR	Mean	-16.8	-10.8	3.9	17.8	22.7	16.9	2.8	-10.9
		SD	4.3	3.4	1.2	2.7	2.5	2.8	1.3	3.6
	Lateral tilt	Mean	5.7	2.6	0.3	-4.4	-7.0	-5.1	0.7	5.2
		SD	3.9	1.4	0.9	4.4	6.0	3.8	1.0	3.7
Reference Study	A/P tilt	Mean	-0.7	10.2	16.6	9.0	-0.4	-8.8	-12.2	-8.2
		SD	1.6	1.4	1.3	1.2	1.6	2.3	2.4	2.2
	AR	Mean	-12.0	-4.6	2.8	12.5	19.7	14.9	4.1	-9.3
		SD	1.9	1.8	1.3	1.4	1.4	1.4	1.2	1.7
	Lateral tilt	Mean	6.0	4.8	-1.6	-7.5	-8.3	-2.7	-0.2	1.7
		SD	1.0	1.1	0.7	1.0	8.3	1.0	0.7	0.8
Difference	A/P tilt	Mean	1.8	5.6	2.7	4.6	-1.1	-4.1	-4.3	-4.1
	AR	Mean	-4.8	-6.2	1.1	5.3	3.0	2.0	-1.3	-1.6
	Lateral tilt	Mean	-0.3	-2.2	1.9	3.1	1.3	-2.4	0.9	3.5

The calculated differences are inserted for all the three rotations to SPSS and statistically compared to the mean value of zero. According to the one sample T-test results, there are no evidences of significant differences between the data gathered using checkerboard and data demonstrated in the reference study. Accordingly, test results for Anteroposterior tilt (test value = 0.156, $p = 0.880$), Axial rotation (test value = -0.570, $p = 0.584$), and Lateral tilt (test value = 0.847, $p = 0.421$) are collected.

In order to test the consistency and reliability of measurement between the 10 subjects, results of the measurements for each participant, at each marker, and in all three orientations of the neck was tested using Cronbach's alpha. For the necessary calculations, Minitab software (version 20.4) was used. Accordingly, Table 9 represents the Cronbach's alpha calculated for this experiment.

Table 9: Cronbach's Alpha of Neck Orientation

Orientation	**Cronbach's Alpha**
A/P tilt	0.995
AR	0.996
Lateral Tilt	0.941

After conducting the validity experiment with 10 participants each at 3 blocks of random 8 directions 240 samples were collected for each orientation of the neck. In the following the necessary calculation of the sample size using Yamane's method, and the power of the one sample T-test is provided. According to Islam (2018), for population size > 100000, and at the precision of ±10%, 100 samples are required. Furthermore, reducing the precision value to ±7%, ±5%, and ±3% would result on bigger sample sizes of 204, 400, and 1111 participants, respectively. Furthermore, in order to calculate the power of the one Sample T-test, Minitab software was used. Table 10 represents descriptive characteristics of the experiment measurements.

Table 10: Data Descriptive

Direction	n	Mean	SD	Standard Error	95% CI
A/P tilt	10	0.20	3.81	1.27	(-2.73, 3.13)
AR	10	-0.74	3.87	1.29	(-3.71, 2.24)
Lateral tilt	10	0.23	1.01	0.34	(-0.54, 1.00)

For the calculation of the test power, sample size and SDs for each orientation of neck was inserted into the software. According to Minitab (2021), the "Differences" argument required for power calculation of one sample T-test, defined as the smallest value of precision that has practical consequences. Hence, in order to provide a comprehensive information with regards to test power of the experiment, a range of Differences' values are provided in table 11 with their respective power test.

Table 11: Power of the One Sample T-test

Orientation	n	SD	Differences				
			1°	2°	3°	4°	5°
A/P tilt	10	3.81	0.11	0.31	0.60	0.84	0.96
AR	10	3.87	0.11	0.31	0.59	0.83	0.95
Lateral tilt	10	1.01	0.79	>0.99	>0.99	>0.99	>0.99

Chapter 5

DISCUSSION

Based on the findings provided in the Results chapter, the algorithm successfully measured 6 DF information of every checkerboard in the video frame. Attaching checkerboards to the human body in different setup combinations gives the algorithm the advantage of providing detailed information about different body segment orientations. Moreover, in comparison with traditional methods such as REBA and RULA, rather than assessing human position based on the most awkward or static posture, the algorithm is capable of providing objective values continuously with high precision (Hignett & McAtamney, 2000; McAtamney & Corlett, 1993; Namwongsa et al., 2018).

According to the result of the precision experiment, overall, the algorithm can measure the 3D location with 19.19 mm precision and the 3D orientation with 5.10° precision. The precision values are calculated based on the standard deviation of the total experiment without considering the effect of the independent factors. Considering the best outcome of the experiment, where the checkerboard pattern is set to 6×7-10mm, the data get significantly more precise to the values of 15.88mm for location and 2.88° for orientation. Since the algorithm includes a zeroing step for initialization of the posture tracking, any value assigned to it will be considered as the true value of the checkerboards' location and orientations. Therefore, the precision could be a good indicator of the measurement accuracy as well. In comparison with the EMT device in

Balaraman et al. (2018) study, lower accuracy was achieved. Furthermore, the precision of state-of-the-art EMT devices is presented by Root Mean Square values. In order to provide the equivalent values, the study conducted by Suzuki et al. (2019) used FASTRACK EMTs and according to the data provided by the company, the static precision of the mentioned device is 0.76mm Root Mean Square Error (RMSE) in location and 0.15° RMSE in orientation (Polhemus, 2022). Overall RMSE of the proposed algorithm is 9.87mm in location and 3.15° in orientation. Considering the best checkerboard pattern, RMSE of 7.07 for location and 2.06 for orientation are achieved.

Compared to the EMT trackers, less precise information is expected from the algorithm. However, less hardware dependency and cost-effectiveness of this algorithm can make it useful for many non-clinical ergonomics studies as well as real-life applications in both industrial and computer workstation posture analysis.

Both location and orientation precisions can be affected significantly by the pattern of the checkerboards ($p < 0.005$). Accordingly, the more the number of rows and columns and the bigger the size of the squares, the higher precision is expected in the measurements. But the size of the checkerboards is limited to the location of attachment and type of the task. Histograms of measurement errors provided in the appendix section of this study also demonstrate much detailed information about the factors which are affecting the consistency of the measurement. In order to be more specific, in appendix B which is related to the distribution of the location error from the true value, a higher number of corner points present more reliability in the measurement of the constant objects. Moreover, the higher number of corner points reduces the chance of extreme outlier values. For instance, comparing 4×5-08mm with

6×7-08mm checkerboard patterns, it is clear that the latter corner point pattern shows a more precise measurement for location. Similarly, more spread data points are observable for the lower number of corner points in the orientation measurement histograms of appendix C. Another factor that shows to some extent a positive contribution to the precision of both location and orientation is the size of the squares of the checkerboard pattern. Based on appendices B and C, the bigger the size of the checkerboard squares the more precise measurement is expected. A similar result can be observed on the box plot provided in figure 18.

Even though the corner point pattern factor played a significant role in the precision of the measurement, the resolution factor shows a more randomized outcome in this study (see appendix D, and Figure 19). As supporting evidence, the Kruskal-Wallis test shows an insignificant difference between the data distribution based on the resolution in location precision. Significantly less reliable measurements are observable in the precision orientation measurement at 4000×3000 resolution ($p = 0.112$). No rational or clear reasoning is available for such abnormality related to this spike but it is suspected that heavy data compression applied to the video frames inside the video camera caused the lower precision at this frame resolution. This yet is not supported by any data and more investigation is required for any definitive conclusion. Generally, with the current setup of the experiment, it is recommended to select a lower chosen resolution since it has a limited effect on the precision of the measurement and it takes less computation time to detect the checkerboards per frame.

In addition to the pattern and the resolution, axes measurement precisions differed significantly in both orientation and location. As illustrated in Figure 20 and Appendix E the algorithm measured the x and y axes' location significantly more precise than the

z-axis ($p < 0.005$). Based on the reference plane setup, this axis is pointed towards the camera direction, providing information regarding the depth of the 2D image. To be more specific, the reference checkerboard in the experiment was positioned in front of the camera and the z-axis of the camera and reference plane were parallel. On the contrary, the z-axis was found to be the most precise one in orientation measurements. According to the methodology chapter, during the selection process of the corner point patterns, the asymmetricity of the pattern was taken into account and according to the finding of the precision experiment, the algorithm successfully was capable of measuring 360 degrees of orientation in the z-axis with high precision.

As mentioned in the second chapter of this thesis, other alternative methods have been utilized to continuously track human posture in the literature. Therefore, in the following necessary comparison between the proposed algorithm and such alternatives are provided.

One of the methods to continuously track the body posture is to use digital or electronic inclinometers (Afshari *et al.*, 2014; Palm, 2017; Paquet, Punnett, & Buchholz, 2001). While such devices are capable of providing accurate measurement of the body joint angles, attachment and assessment of the data are challenging (Palm, 2017). Moreover, each inclinometer is capable of providing from 1 to 3 DF information with regards to orientation only. Not to mention the high cost of purchasing such devices, the proposed method of this study is capable of providing extra information regarding the 3D location of its markers, and there is no need for cable routing in the subjects' body. However, it should be mentioned that the digital inclinometers are capable of providing more accurate orientation measurements.

The second option for continuous posture analysis is the Computer-assisted Recording and Long-term Analysis of Musculoskeletal Loads (CUELA) measuring systems (Ellegast, Hermanns, & Schiefer, 2009). This wearable device not only is capable of capturing 3D motion of the trunk, but also can detect the heavy workloads lifted by the individuals using pressure sensors located at the bottom of their feet. All the data is logged inside the memory card and after the action is transferred to a computer for further analysis. CUELA is suitable for continuously tracking the motion of the subject especially in the trunk and lower extremity areas. However, it cannot provide sufficient information about majority of joints located in upper extremity region, namely shoulders, arms, wrists, and neck. Even though, both CUELA measurement systems and the proposed algorithm can provide useful information with regards to continuous posture tracking, each provide different types of information that cannot be directly compared. No information regarding the weight of an object can be provided by the proposed algorithm while CUELA is capable of providing accurate information in this regard using pressure sensors (Ellegast *et al.*, 2009). On the other hand, CUELA lacks the necessary information about the axis of rotation of the joints and can only provide a single angle of rotation.

Another alternative to continuously track human body posture is to use the Body Area Network system. While such devices are capable of providing accurate representation of the human body, the focus of their application is on the entertainment industry and human body gesture simulation. There have been several studies utilizing these wireless sensors for posture tracking and posture analysis in the field of ergonomics (Dong *et al.*, 2015; Sivanathan, 2014; Valero *et al.*, 2017). One of the benefits of this method is the small sized tracking markers that can be attached on body parts with low

surface for installments. Small tracking markers are mainly used for capturing facial expression of a person in details. However, one of the useful applications of these sensor in the field of ergonomics is to track the small body parts such as fingers. Although such small sensor and fast calculation of 3D position of each tracker, thanks to triangulation technique, gives this technique an edge compared to the developed algorithm, the method requires multiple cameras and can only represent the 3D location of the markers and no information about the orientation. The latter drawback consequently can only represent a single angle of orientation on the body joints which may not be sufficient in particular cases.

One more marker-less and affordable alternative which, is used in several studies, is the Microsoft Kinect device (Abobakr *et al.*, 2017; Han *et al.*, 2013; Khosrowpour *et al.*, 2014). Similar to the Body Network Area method, this device and similar RGB-D devices are only capable of showing a single angle of orientation for the joint. Also, although affordable, such devices require specific camera equipment to be purchase while, the developed algorithm can use cell phone camera as the main source of measurement.

Last but not least, EMTs are capable of providing 6 DF information similar to the developed algorithm faster, with more resolution in terms of data per second, more accurately, and more precisely (Cerrito *et al.*, 2018; Kellermeier *et al.*, 2017). But, the cost of using this method in comparison with the proposed algorithm is significantly higher. Generally, the cost factor is an important indicator of the advantage of the proposed algorithm which can open more opportunity for the researchers to conduct their study cheaper with acceptable precision.

One of the potentials of using this algorithm can be in the computer workstation where the majority of body movements are located in the upper extremity. For example, determining the angle keyboard levitation for ergonomic design of a keyboard or the mouse tilt angle and its effect on prevention of forearm pronation can be measured by attaching markers on the upper arm, forearm, and posterior part of the hand and recording video of the participant in a top-down angle view.

Another potential of the algorithm in the computer workstation could be measuring different neck orientations namely, anteroposterior tilt, axial rotation, and lateral tilt and its correlation with the position and the size of the monitor. Attaching the checkerboard markers similar to the validity experiment of this study can provide results no different than EMTs, but with less precision.

Finally, it is good to mentioned that the algorithm was capable of providing similar result, at a lower precision, to the experiment conducted by Roby-Brami *et al.* (2020).

It can be argued that in the field of ergonomics, such accurate measurement is not necessary and visual estimations are enough to conduct an assessment in the work place. In respond, it can also be argued that designing a product such as chair, mouse, or keyboard ergonomically requires detailed measurement of body segment orientation and such measurements are usually done using expensive equipment. Using the developed method can reduce the cost of product design effectively which consequently results in more affordable ergonomic products in the market. Moreover, the developed algorithm gives more researchers in the field of ergonomics the accessibility of continuous 6 DF information regarding human posture which increases the potential of progress and development of new continuous posture analyses

methods. The importance of the latter arguments can be supported by the study conducted by Bao *et al.* (2007) which investigated the difference between event-based and time-based measurement of the RULA method on 733 subjects. According to their findings, the results of the assessments were not cohesive and there were differences in measurement between event-based and time-based methods.

Representing 6 DF of information, give the algorithm an edge in comparison with its competitors (Buzzi et al., 2017; Dang et al., 2017; Jones et al., 2016; Seo et al., 2019; Wang et al., 2018). To be more specific, techniques such as REBA and RULA which require 6 DF information to analyze human postures, can be utilized on the algorithm to track the posture continuously during different job tasks (Hignett & McAtamney, 2000; McAtamney & Corlett, 1993).

5.1 Limitation of the Study

As discussed in the methodology chapter, having enough light for capturing the video is an essential part of the experiment. And in the environment where light is limited, noise and motion blur will be introduced to the captured footage. The mentioned parameters can affect the accuracy and precision of the measurement and other approaches should be considered in such an environment. Higher-end cameras and lenses which are capable of recording in low light conditions can be utilized for measurement. But it would make this approach costly for analysis and devices such as EMT would be more suitable. On the other hand, in comparison with other methods such as RGB-D, and Microsoft Kinect, where the outdoor environment is a negative factor for measurement, the proposed method can have an edge in capturing video frames in environments with high light exposure namely outdoor places and construction zones (Ahmed Abobakr et al., 2019). Thanks to the well-lit frame,

aperture, ISO, and shutter speed of the video camera can be adjusted in favor of a sharper image for corner point detection.

Another limitation of this algorithm is the intensive computations. During the experiment, it was observed that the time of computation heavily depends on the video resolution, number of checkerboards, and computer hardware available for the analysis. In order to reduce the time of calculation for analysis, it is necessary to reduce the time of calculation per frame to a portion of a second.

Moreover, attaching the checkerboard markers to body parts can limit the freedom of movement. For tasks where freedom of movement is an essential part, utilizing this method is not appropriate.

Finally, being limited to a single point of view, this algorithm cannot correctly measure checkerboards at extreme orientations or blocked an object. It should be mentioned that such problems are possible in observational approaches as well (Trask, Mathiassen, & Rostami, 2015). To compensate for this limitation, as a future study, stereo camera techniques can be applied. Accordingly, rather than observing the checkerboard from a single point of view, multiple cameras could be utilized at different locations and orientations to track the target participant at a higher range of movements. For example, if the participant requires to turn away from the camera during a specific job task, the second camera could be positioned behind the subject to eliminate the loss of track of the checkerboards attached to the body of the subject.

5.2 Future Work

Commonly available cell phone devices in recent years' market are capable of recording video with at least 24 frames per second in good resolutions and some of the more advanced devices can also record 120 or 240 frames per second. Each frame recorded as a video can be a timestep of measurement and being able to measure body position 120 and 240 times in one second can also extend the usage of the algorithm for sports industries.

Detecting the checkerboard patterns in the video frames is a time-consuming task and depending on the number of checkerboards to be detected as well as the video resolution and the computer hardware, each frame may require more than one minute of computation in worst-case scenarios. However, after the detection, the entire PnP computations, 3D basis transformation, Euclidean to quaternion transformation, quaternion to Euclidean transformation, and 6 DF data extraction could be calculated in fractions of a second. Therefore, as a future study, utilizing the Convolutional Neural Network (CNN) method and Graphical Processing Unit GPU computation for checkerboard detection could reduce the processing time of the entire algorithm down to less than a second. Consequently, CNN can shift the current state of the algorithm from a post-action assessment method to a live assessment method. Especially because common limitations of the algorithm are the perspective range of camera observation and extreme angles of the checkerboard, the live assessment method can give the researchers the advantage to hold and navigate the camera in person and get a live reading of the body angles at any position. Furthermore, other approaches such as narrowing down the location of each checkerboard in the current frame, for the next frame would reduce the algorithm search for the same checkerboard in the next frame

significantly. For instance, if a checkerboard is located at x and y pixel coordinates in a frame, given the entire size of the checkerboard with a certain offset due to checkerboard movement, this algorithm can search only in the expected location area on the next frame rather than the entire frame. Narrowing down the expected location of the checkerboard in the frame also has the advantage of reducing the probability of miss detection since many objects in a frame could represent a checkerboard-like pattern. This, however, might cost even more computation power to analyze the mentioned offset, and thus, defeat the main purpose of reducing the total process time per frame.

Chapter 6

CONCLUSION

Based on the result achieved in this study, given the right condition such as light and job task specifications, this cost-effective marker-based algorithm can be utilized as a tool for 3D postural analysis and posture tracking with acceptable precision. In comparison with other similar methods, this algorithm can be implemented without the need for advanced utilities at a much lower cost. Thus, it could be a reasonable tool to be considered for future studies.

According to the outcomes of the first experiment, the checkerboard pattern significantly affects the precision of both location and orientation ($p < 0.001$). Using the PnP technique to extract 6 DF information favors a greater number of corner points on each marker. Similarly, the size of the checkerboards plays an important role in achieving significantly higher accuracy in both location and orientation measurements ($p < 0.05$).

The effect of video resolution on the orientation precision is significant ($p = 0.005$). To be more specific, comparing the resolution of 2560×1920, and 3200×2400 with 4000×3000 they show significantly higher precision measurements ($p < 0.005$). The same conclusion does not hold for the location precision on this factor.

The precision of the location and orientation measurement significantly varies based on the axis at which the information is extracted ($p < 0.001$). Regarding the orientation precision, values measured along the z-axis are more precise than values measured along the x and y axes ($p < 0.001$). On the contrary, regarding the location precision, location precision was found to be much lower along the z-axis compared to other axes ($p < 0.001$). Therefore, during the experimental design attaching the markers to the body segments requires the examiners' attention.

Related to the type II error and power test calculations, the corner point pattern factor shows a power test of more than 99% for both the location and the orientation. The resolution factor, on the other hand, shows an extremely high value for type II error (> 99%) for both location and orientation. This indicates the lack of enough evidence for any conclusive decision on this factor. Regarding the axes factor, power tests of 97% and >99% are measured for the location and orientation precision, respectively.

Finally, according to the outcome of the study, the measurement although less precise does not significantly differ from the other common methods such as using EMTs ($p > 0.4$). Postural analysis in the field of ergonomics plays a vital role. Additionally, the bad implementation of job tasks in the working environment without considering the human body restrictions put employees in the danger of prolonged musculoskeletal disorders. Therefore, in order to eliminate the prevalence of such discomforts, further studies are necessary. Making the assessment methods of posture analysis more reachable to the hand of researchers could be a good initiative to encourage scientists in the field of ergonomics to devote more time to detecting risk factors and providing a better solution to the common challenges in the industry. Hence, providing solutions such as the algorithm of this study could help with the matter.

Considering all the limitations of the proposed technique, the algorithm is capable of continuously tracking the posture of the subjects at reasonable precision and providing 6 DF information several times a second. The frequency and type of the data provided by this approach may open many opportunities for future assessment techniques of 3D postural tracking as well.

According to the precision experiment of the study, many factors can make or break the process of posture tracking using this algorithm. Hence, deciding on the measurement approach and considering factors such as environment, marker, and video specifications are very crucial to achieving a desirable outcome. Therefore, it would be very helpful to understand and narrow down what exactly need to be measured, and what type of movement is expected to implement the algorithm properly. For instance, bigger sizes of checkerboards can be used if the intended purpose is to measure the orientation of the hips in comparison with the wrist.

With recent technological advancements and the shift of industries towards automation and industry 4.0, many of the common tasks are being handled with software and computer programs. Therefore, the authors hope this algorithm would contribute to the ergonomic-related research and further analysis of human body posture, especially in computer workstations.

REFERENCES

Abobakr, A., Nahavandi, D., Hossny, M., Iskander, J., Attia, M., Nahavandi, S., & Smets, M. (2019). RGB-D ergonomic assessment system of adopted working postures. *Applied ergonomics*, 80, 75-88.

Abobakr, A., Nahavandi, D., Iskander, J., Hossny, M., Nahavandi, S., & Smets, M. (2017, 5-8 Oct. 2017). RGB-D human posture analysis for ergonomie studies using deep convolutional neural network. In *Proceedings of the 2017 IEEE International Conference on Systems, Man, and Cybernetics (SMC)*.

Afshari, D., Mohammadi, A., Saki, A., & Movafaghpour, M. (2014). Continuous monitoring of back postures using portable inclinometer among nursing assistants. *Iran Occupational Health*, 11(3), 30-39.

Ahmed, E., Jones, M., & Marks, T. K. (2015). An improved deep learning architecture for person re-identification. In *Proceedings of the IEEE conference on computer vision and pattern recognition*.

Al Madani, D., & Dababneh, A. (2016). Rapid entire body assessment: A literature review. *American Journal of Engineering and Applied Sciences*, 9(1), 107-118.

Alsadik, B. (2016). A modified method for image triangulation using inclined angles. *International Archives of the Photogrammetry, Remote Sensing & Spatial Information Sciences*, 41.

Alwasel, A., Elrayes, K., Abdel-Rahman, E., & Haas, C. (2013). A human body posture sensor for monitoring and diagnosing MSD risk factors. In *Proceedings of the International Symposium on Automation and Robotics in Construction*, Monteal, QC.

Baker, W. D., & Mansfield, N. J. (2010). Effects of horizontal whole-body vibration and standing posture on activity interference. *Ergonomics,* 53(3), 365-374.

Balaraman, S., Chakrabarti, A., Gurumoorthy, B., & Sen, D. (2018). Automated identification of distinct events in an assembly process using tracking of body postures. *Concurrent Engineering-Research and Applications,* 26(2), 198-207. doi:10.1177/1063293x17745941

Bao, S., Howard, N., Spielholz, P., & Silverstein, B. (2007). Two posture analysis approaches and their application in a modified rapid upper limb assessment evaluation. *Ergonomics,* 50(12), 2118-2136.

Bar-Itzhack, I. Y. (2000). New method for extracting the quaternion from a rotation matrix. *Journal of guidance, control, and dynamics,* 23(6), 1085-1087.

Beveridge, R. (2014). *Trigonometry*: Self.

Bhatt, N., & Skm, V. (2018). Posture similarity index: a method to compare hand postures in synergy space. *Peerj,* 6, e6078. doi:10.7717/peerj.6078

Brodie, D., & Wells, R. (1997). An evaluation of the utility of three ergonomics checklists for predicting health outcomes in a car manufacturing environment. In *Proceedings of the 29th Annual Conference of the Human Factors Association of Canada*.

Buchholz, B., Paquet, V., Punnett, L., Lee, D., & Moir, S. (1996). PATH: a work sampling-based approach to ergonomic job analysis for construction and other non-repetitive work. *Applied ergonomics,* 27(3), 177-187.

Buzzi, J., Gatti, C., Ferrigno, G., & De Momi, E. (2017). Analysis of joint and hand impedance during teleoperation and free-hand task execution. *Ieee Robotics and Automation Letters,* 2(3), 1733-1739. doi:10.1109/lra.2017.2678546

Cerrito, A., Milburn, P., Adams, R., & Evans, K. (2018). Cervical spine kinematics measured during rugby union scrums: Reliability of optoelectronic and electromagnetic tracking systems. *Cogent Medicine,* 5(1), 1526758.

Cipolla, R., Battiato, S., & Farinella, G. M. (2010). *Computer vision: Detection, recognition and reconstruction* (Vol. 285): Springer.

Dang, D. C., Dang, Q. K., Chee, Y. J., & Suh, Y. S. (2017). Neck flexion angle estimation during walking. *Journal of Sensors,* 2017, 1-9. doi:10.1155/2017/2936041

Dartt, A., Rosecrance, J., Gerr, F., Chen, P., Anton, D., & Merlino, L. (2009). Reliability of assessing upper limb postures among workers performing manufacturing tasks. *Applied ergonomics*, 40(3), 371-378.

Dockrell, S., O'Grady, E., Bennett, K., Mullarkey, C., Mc Connell, R., Ruddy, R., . . . Flannery, C. (2012). An investigation of the reliability of Rapid Upper Limb Assessment (RULA) as a method of assessment of children's computing posture. *Applied ergonomics*, 43(3), 632-636.

Dong, Z., Gu, H., Wan, Y., Zhuang, W., Rojas-Cessa, R., & Rabin, E. (2015, 9-11 April 2015). Wireless body area sensor network for posture and gait monitoring of individuals with Parkinson's disease. In *Proceedings of the 2015 IEEE 12th International Conference on Networking, Sensing and Control*.

Ellegast, R., Hermanns, I., & Schiefer, C. (2009). Workload assessment in field using the ambulatory CUELA system. In *Proceedings of the International Conference on Digital Human Modeling*.

Fischler, M. A., & Bolles, R. C. (1981). Random sample consensus: A paradigm for model fitting with applications to image analysis and automated cartography. *Communications of the ACM*, 24(6), 381-395.

Fu, K. S. (2004). IEEE transactions on pattern analysis and machine intelligence. In S. Kotz, C. B. Read, N. Balakrishnan, B. Vidakovic, & J. N.L. (Eds.), *Encyclopedia of Statistical Sciences*. Hoboken, New Jersey, United States: John Wiley & Sons, Inc.

Gao, X.-S., Hou, X.-R., Tang, J., & Cheng, H.-F. (2003). Complete solution classification for the perspective-three-point problem. *IEEE Transactions on pattern analysis and machine intelligence,* 25(8), 930-943.

Gascon, S. S., Gilmer, G. G., Hanks, M. M., Washington, J. K., & Oliver, G. D. (2018). Biomechanical influences of a postural compression garment on scapular positioning. *International Journal of Sports Physical Therapy,* 13(4), 700-706. doi:10.26603/ijspt20180700

Geiger, A., Moosmann, F., Car, Ö., & Schuster, B. (2012). Automatic camera and range sensor calibration using a single shot. In *Proceedings of the 2012 IEEE International Conference on Robotics and Automation*, St Paul, MN.

Geisbüsch, A., Auer, C., Dickhaus, H., Putz, C., & Dreher, T. (2017). Electromagnetic tracking for femoral derotation osteotomy—an in vivo study. *Journal of Orthopaedic Research,* 35(12), 2652-2657. doi:https://doi.org/10.1002/jor.23579

Geisbüsch, A., Götze, M., Putz, C., Dickhaus, H., & Dreher, T. (2021). Femoral derotation osteotomy—Does intraoperative electromagnetic tracking reflect the dynamic outcome? *Journal of Orthopaedic Research,* 40(6). doi:https://doi.org/10.1002/jor.25168

Golchha, V., Sharma, P., Wadhwa, J., Yadav, D., & Paul, R. (2014). Ergonomie risk factors and their association with musculoskeletal disorders among Indian

dentist: A preliminary study using rapid upper limb assessment. *Indian journal of dental research*, 25(6).

Gold, J., Driban, J., Yingling, V., & Komaroff, E. (2012). Characterization of posture and comfort in laptop users in non-desk settings. *Applied ergonomics*, 43(2), 392-399.

Grobler, S. H., Mostert, K., & Becker, P. (2018). The impact of a change in work posture from seated to stand-up on work-related musculoskeletal disorders among sewing-machine operators. *American Journal of Industrial Medicine*, 61(8), 699-711. doi:10.1002/ajim.22865

Guichard, D., Bailey, J., Blenkinsop, M., Cavers, M., Hartman, G., & J., L. (2020). *Calculus: Early transcendentals*. Calgary, Canada: Lyryx Learning Inc.

Habechian, F. A. P., Rosa, D. P., Haik, M. N., & Camargo, P. R. (2016). Sex-related differences in scapular kinematics during elevation of the arm in asymptomatic children and adults. *Journal of Applied Biomechanics*, 32(5), 513-519. doi:10.1123/jab.2015-0341

Han, S., Achar, M., Lee, S., & Peña-Mora, F. (2013). Empirical assessment of a RGB-D sensor on motion capture and action recognition for construction worker monitoring. *Visualization in Engineering*, 1(1), 6.

Hartley, R., & Zisserman, A. (2003). *Multiple view geometry in computer vision*. Cambridge (England): Cambridge university press.

Hartley, R. I., & Sturm, P. (1995). Triangulation. In *Proceedings of the International Conference on Computer Analysis of Images and Patterns*.

Hartley, R. I., & Sturm, P. (1997). Triangulation. *Computer vision and image understanding*, 68(2), 146-157.

Heikkila, J., & Silven, O. (1997). A four-step camera calibration procedure with implicit image correction. In *Proceedings of the cvpr*, San Juan, PR.

Hignett, S., & McAtamney, L. (2000). Rapid entire body assessment (REBA). *Applied ergonomics*, 31(2), 201-205.

Hoppes, C. W., Sparto, P. J., Whitney, S. L., Furman, J. M., & Huppert, T. J. (2018). Changes in cerebral activation in individuals with and without visual vertigo during optic flow: A functional near-infrared spectroscopy study. *Neuroimage-Clinical*, 20, 655-663. doi:10.1016/j.nicl.2018.08.034

Islam, M. R. (2018). Sample size and its role in Central Limit Theorem (CLT). *Computational and Applied Mathematics Journal*, 4(1), 1-7.

ISO 5800:1987(en) Photography — Colour negative films for still photography — Determination of ISO speed. (2016). 2. Retrieved from https://www.iso.org/obp/ui/#iso:std:iso:5800:ed-2:v1:en

Jackson, J. A., Mathiassen, S. E., & Liv, P. (2016). Observer performance in estimating upper arm elevation angles under ideal viewing conditions when assisted by posture matching software. *Applied ergonomics*, 55, 208-215.

Janesick, J. R. (2001). *Scientific charge-coupled devices* (Vol. 83): SPIE press.

Jones, G. D., James, D. C., Thacker, M., & Green, D. A. (2016). Sit-to-stand-and-walk from 120% knee height: A novel approach to assess dynamic postural control independent of lead-limb. *Jove-Journal of Visualized Experiments*(114), 1-17. doi:10.3791/54323

Karhu, O., Kansi, P., & Kuorinka, I. (1977). Correcting working postures in industry: a practical method for analysis. *Applied ergonomics*, 8(4), 199-201.

Keller, K., Kampfer, H., Matejec, R., Lapp, O., Krafft, W., Frenken, H., . . . Ketellapper, L. (2000). Photography. In *Ullmann's Encyclopedia of Industrial Chemistry*.

Kellermeier, M., Herbolzheimer, J., Kreppner, S., Lotter, M., Strnad, V., & Bert, C. (2017). Electromagnetic tracking (EMT) technology for improved treatment quality assurance in interstitial brachytherapy. *Journal of Applied Clinical Medical Physics*, 18(1), 211-222. doi:https://doi.org/10.1002/acm2.12021

Khosrowpour, A., Fedorov, I., Holynski, A., Niebles, J. C., & Golparvar-Fard, M. (2014). Automated worker activity analysis in indoor environments for direct-work rate improvement from long sequences of RGB-D images. In

Proceedings of the Construction Research Congress 2014: Construction in a Global Network.

Kobayashi, K., Gransberg, L., Knutsson, E., & Nolen, P. (1997). A new system for three-dimensional gait recording using electromagnetic tracking. *Gait & Posture,* 6(1), 63-75.

Kumar, V. K., Kumar, S. P., & Baliga, M. R. (2013). Prevalence of work-related musculoskeletal complaints among dentists in India: a national cross-sectional survey. *Indian journal of dental research,* 24(4), 428.

Learman, K. E., Benedict, J. A., Ellis, A. R., Neal, A. R., Wright, J. A., & Landgraff, N. C. (2016). An exploration of trunk reposition error in subjects with acute stroke: An observational design. *Topics in Stroke Rehabilitation,* 23(3), 200-207. doi:10.1080/10749357.2016.1138671

Lee, Y.-J., & Park, M.-W. (2019). 3D tracking of multiple onsite workers based on stereo vision. *Automation in Construction,* 98, 146-159.

Lemmers, G. P. G., Heijmans, M. W. M., Scafoglieri, A., Buyl, R., Staal, J. B., Schmitt, M. A., & Cattrysse, E. (2018). Three-dimensional kinematics of the cervical spine using an electromagnetic tracking device. Differences between healthy subjects and subjects with nonspecific neck pain and the effect of age. *Clinical Biomechanics,* 54, 111-117. doi:10.1016/j.clinbiomech.2018.03.012

Li, S., Xu, C., & Xie, M. (2012). A Robust O(n) solution to the perspective-n-point problem. *IEEE Transactions on pattern analysis and machine intelligence,* 34(7), 1444-1450. doi:10.1109/TPAMI.2012.41

Liu, M., Han, S., & Lee, S. (2016). Tracking-based 3D human skeleton extraction from stereo video camera toward an on-site safety and ergonomic analysis. *Construction Innovation*.

Mani, R., Milosavljevic, S., & Sullivan, S. J. (2015). Control of posture during tasks representing common work-related postures–a reliability study. *Ergonomics,* 58(6), 980-989.

Masaki, M., Tateuchi, H., Koyama, Y., Sakuma, K., Otsuka, N., & Ichihashi, N. (2018). Back muscle activity and sagittal spinal alignment during quadruped upper and lower extremity lift in young men with low back pain history. *Gait & Posture,* 66, 221-227. doi:10.1016/j.gaitpost.2018.09.002

MATLAB. (2013). extrinsics. Retrieved from https://www.mathworks.com/help/vision/ref/extrinsics.html

MATLAB. (2017). Single camera calibrator app. Retrieved from https://www.mathworks.com/help/vision/ug/single-camera-calibrator-app.html

MATLAB. (2018a). detectCheckerboardPoints. Retrieved from https://www.mathworks.com/help/vision/ref/detectcheckerboardpoints.html

MATLAB. (2018b). undistortImage. Retrieved from https://www.mathworks.com/help/vision/ref/undistortimage.html

McAtamney, L., & Corlett, E. N. (1993). RULA: a survey method for the investigation of work-related upper limb disorders. *Applied ergonomics,* 24(2), 91-99.

Minitab. (2021). Enter your data for power and sample size for 1-Sample T. Retrieved from https://support.minitab.com/en-us/minitab/20/help-and-how-to/statistics/power-and-sample-size/how-to/hypothesis-tests/power-and-sample-size-for-1-sample-t/perform-the-analysis/enter-your-data/?SID=27300

Montgomery, D. C. (2017). *Design and analysis of experiments*: John wiley & sons.

Moseley, L., Smith, R., Hunt, A., & Gant, R. (1996). Three-dimensional kinematics of the rearfoot during the stance phase of walking in normal young adult males. *Clinical Biomechanics,* 11(1), 39-45.

Namwongsa, S., Puntumetakul, R., Neubert, M. S., Chaiklieng, S., & Boucaut, R. (2018). Ergonomic risk assessment of smartphone users using the Rapid Upper Limb Assessment (RULA) tool. *PloS one,* 13(8), e0203394.

Nazerian, R. (2016). *Work related musculoskeletal discomfort among Iranian heavy truck drivers.* Eastern Mediterranean University (EMU)-Doğu Akdeniz Üniversitesi (DAÜ),

Nazerian, R., Korhan, O., & Shakeri, E. (2018). Work-related musculoskeletal discomfort among heavy truck drivers. *International Journal of Occupational Safety and Ergonomics,* 26(2), 233-244. doi:10.1080/10803548.2018.1433107

Nguyen, P. B., Kang, B., Bappy, D. M., Choi, E., Park, S., Ko, S. Y., . . . Kim, C. S. (2018). Real-time microrobot posture recognition via biplane X-ray imaging system for external electromagnetic actuation. *International Journal of Computer Assisted Radiology and Surgery,* 13(11), 1843-1852. doi:10.1007/s11548-018-1846-z

Nutt, J. G., Bloem, B. R., Giladi, N., Hallett, M., Horak, F. B., & Nieuwboer, A. (2011). Freezing of gait: moving forward on a mysterious clinical phenomenon. *The Lancet Neurology,* 10(8), 734-744. doi:https://doi.org/10.1016/S1474-4422(11)70143-0

Occhipinti, E., & Colombini, D. (1996). Proposal of a concise index for the evaluation of the exposure to repetitive movements of the upper extremity (OCRA index). *La Medicina del lavoro,* 87(6), 526-548.

Pal, A., & Dhara, P. C. (2018). Work related musculoskeletal disorders and postural stress of the women cultivators engaged in uprooting job of rice cultivation. *Indian Journal of Occupational and Environmental Medicine,* 22(3), 163-169. doi:10.4103/ijoem.IJOEM_104_18

Palm, P. (2017). *Methods to assess physical load at work: With a focus on the neck and upper extremities.* Acta Universitatis Upsaliensis,

Paquet, V. L., Punnett, L., & Buchholz, B. (2001). Validity of fixed-interval observations for postural assessment in construction work. *Applied ergonomics,* 32(3), 215-224.

Patruno, C., Marani, R., Cicirelli, G., Stella, E., & D'Orazio, T. (2019). People re-identification using skeleton standard posture and color descriptors from RGB-D data. *Pattern Recognition,* 89, 77-90.

Pellegrini, S., & Iocchi, L. (2007). Human posture tracking and classification through stereo vision and 3D model matching. *EURASIP Journal on Image and Video Processing,* 2008, 1-12.

Perera, T., Yohanandan, S. A. C., Thevathasan, W., Jones, M., Peppard, R., Evans, A. H., . . . McDermott, H. J. (2016). Clinical validation of a precision electromagnetic tremor measurement system in participants receiving deep brain stimulation for essential tremor. *Physiological Measurement,* 37(9), 1516-1527. doi:10.1088/0967-3334/37/9/1516

Pillastrini, P., Mugnai, R., Bertozzi, L., Costi, S., Curti, S., Guccione, A., . . . Violante, F. S. (2010). Effectiveness of an ergonomic intervention on work-related posture and low back pain in video display terminal operators: a 3 year cross-over trial. *Applied ergonomics,* 41(3), 436-443.

Plamondon, A., Delisle, A., Larue, C., Brouillette, D., McFadden, D., Desjardins, P., & Larivière, C. (2007). Evaluation of a hybrid system for three-dimensional measurement of trunk posture in motion. *Applied ergonomics,* 38(6), 697-712.

Polhemus. (2022). FASTRACK, the workhorse 6dof motion tracker that set the standard in tracking. . Retrieved from https://polhemus.com/motion-tracking/all-trackers/fastrak/

Rattanaprasert, U., Smith, R., Sullivan, M., & Gilleard, W. (1999). Three-dimensional kinematics of the forefoot, rearfoot, and leg without the function of tibialis posterior in comparison with normals during stance phase of walking. *Clinical Biomechanics,* 14(1), 14-23.

Ren, L., Lu, J., Feng, J., & Zhou, J. (2017). Multi-modal uniform deep learning for RGB-D person re-identification. *Pattern Recognition,* 72, 446-457.

Rezagholi, M., Mathiassen, S. E., & Liv, P. (2012). Cost efficiency comparison of four video-based techniques for assessing upper arm postures. *Ergonomics,* 55(3), 350-360.

Roby-Brami, A., Lefèvre Colau, M.-M., Parry, R., Acapo, S., Rannou, F., & Roren, A. (2020). Orientation of the head and trunk during functional upper limb movement. *Applied Sciences,* 10(6), 2115. Retrieved from https://www.mdpi.com/2076-3417/10/6/2115

Scaramuzza, D., Martinelli, A., & Siegwart, R. (2006). A toolbox for easily calibrating omnidirectional cameras. In *Proceedings of the 2006 IEEE/RSJ International Conference on Intelligent Robots and Systems*, Beijing, China.

Schumann, A., & Stiefelhagen, R. (2017). Person re-identification by deep learning attribute-complementary information. In *Proceedings of the IEEE conference on computer vision and pattern recognition workshops*.

Seo, J., Alwasel, A., Lee, S., Abdel-Rahman, E. M., & Haas, C. (2019). A comparative study of in-field motion capture approaches for body kinematics measurement in construction. *Robotica,* 37(5), 928-946. doi:10.1017/s0263574717000571

Sivanathan, A. (2014). *Ubiquitous Integration and Temporal Synchronisation (UbilTS) framework: a solution for building complex multimodal data capture and interactive systems.* Heriot-Watt University,

Sottimano, I., Viotti, S., Guidetti, G., Cascio, V., & Converso, D. (2018). "I break and bend". Posture, lifts and musculoskeletal disorders among preschool teachers. *Medicina Del Lavoro,* 109(5), 363-374. doi:10.23749/mdl.v110i5.7299

Starbuck, R., Seo, J., Han, S., & Lee, S. (2014). A stereo vision-based approach to marker-less motion capture for on-site kinematic modeling of construction worker tasks. In *Proceedings of the Computing in Civil and Building Engineering, ASCE,* Orlando, FL.

Suzuki, Y., Muraki, T., Sekiguchi, Y., Ishikawa, H., Yaguchi, H., Suzuki, Y., . . . Izumi, S. I. (2019). Influence of thoracic posture on scapulothoracic and glenohumeral motions during eccentric shoulder external rotation. *Gait & Posture,* 67, 207-212. doi:10.1016/j.gaitpost.2018.10.022

Thai, T. H., Cogranne, R., & Retraint, F. (2013). Camera model identification based on the heteroscedastic noise model. *IEEE Transactions on Image Processing*, 23(1), 250-263.

Trask, C., Mathiassen, S. E., & Rostami, M. (2015). Partly visible periods in posture observation from video: prevalence and effect on summary estimates of postures in the job. *Applied ergonomics*, 49, 63-69.

Urban, S., Leitloff, J., & Hinz, S. (2015). Improved wide-angle, fisheye and omnidirectional camera calibration. *ISPRS Journal of Photogrammetry and Remote Sensing*, 108, 72-79.

Valero, E., Sivanathan, A., Bosché, F., & Abdel-Wahab, M. (2016). Musculoskeletal disorders in construction: A review and a novel system for activity tracking with body area network. *Applied ergonomics*, 54, 120-130. doi:https://doi.org/10.1016/j.apergo.2015.11.020

Valero, E., Sivanathan, A., Bosché, F., & Abdel-Wahab, M. (2017). Analysis of construction trade worker body motions using a wearable and wireless motion sensor network. *Automation in Construction*, 83, 48-55. doi:https://doi.org/10.1016/j.autcon.2017.08.001

Vieira, E. R., & Kumar, S. (2004). Working postures: a literature review. *Journal of occupational rehabilitation*, 14(2), 143-159.

Wagner, D. W., Kirschweng, R. L., & Reed, M. P. (2009). Foot motions in manual material handling transfer tasks: A taxonomy and data from an automotive assembly plant. *Ergonomics*, 52(3), 362-383.

Wang, Z. L., Li, J., Wang, J. X., Zhao, H. Y., Qiu, S., Yang, N., & Shi, X. (2018). Inertial sensor-based analysis of equestrian sports between beginner and professional riders under different horse gaits. *Ieee Transactions on Instrumentation and Measurement*, 67(11), 2692-2704. doi:10.1109/tim.2018.2826198

Woodburn, J., Helliwell, P. S., & Barker, S. (2003). Changes in 3D joint kinematics support the continuous use of orthoses in the management of painful rearfoot deformity in rheumatoid arthritis. *The Journal of rheumatology*, 30(11), 2356-2364.

Woodburn, J., Turner, D. E., Helliwell, P. S., & Barker, S. (1999). A preliminary study determining the feasibility of electromagnetic tracking for kinematics at the ankle joint complex. *Rheumatology*, 38(12), 1260-1268. doi:10.1093/rheumatology/38.12.1260

Xu, X., & McGorry, R. W. (2015). The validity of the first and second generation Microsoft Kinect™ for identifying joint center locations during static postures. *Applied ergonomics*, 49, 47-54.

Youyang, F., Qing, W., Yuan, Y., & Chao, Y. (2019). Robust improvement solution to perspective-n-point problem. *International Journal of Advanced Robotic Systems,* 16(6), 1729881419885700.

Zhang, Z. (2000). A flexible new technique for camera calibration. *IEEE Transactions on pattern analysis and machine intelligence,* 22.

Zhou, Z., Wu, B., Duan, J., Zhang, X., Zhang, N., & Liang, Z. (2017). Optical surgical instrument tracking system based on the principle of stereo vision. *Journal of biomedical optics,* 22(6), 065005.

Zhu, X. H., Yurteri-Kaplan, L. A., Cavuoto, L. A., Sokol, A. I., Iglesia, C. B., Gutman, R. E., . . . Paquet, V. (2017). ErgoPART: A computerized observational tool to quantify postural loading in real-time during surgery. *Iise Transactions on Occupational Ergonomics & Human Factors,* 5(1), 23-38. doi:10.1080/24725838.2016.1276032

APPENDICES

Appendix A: Flow Chart of the Algorithm

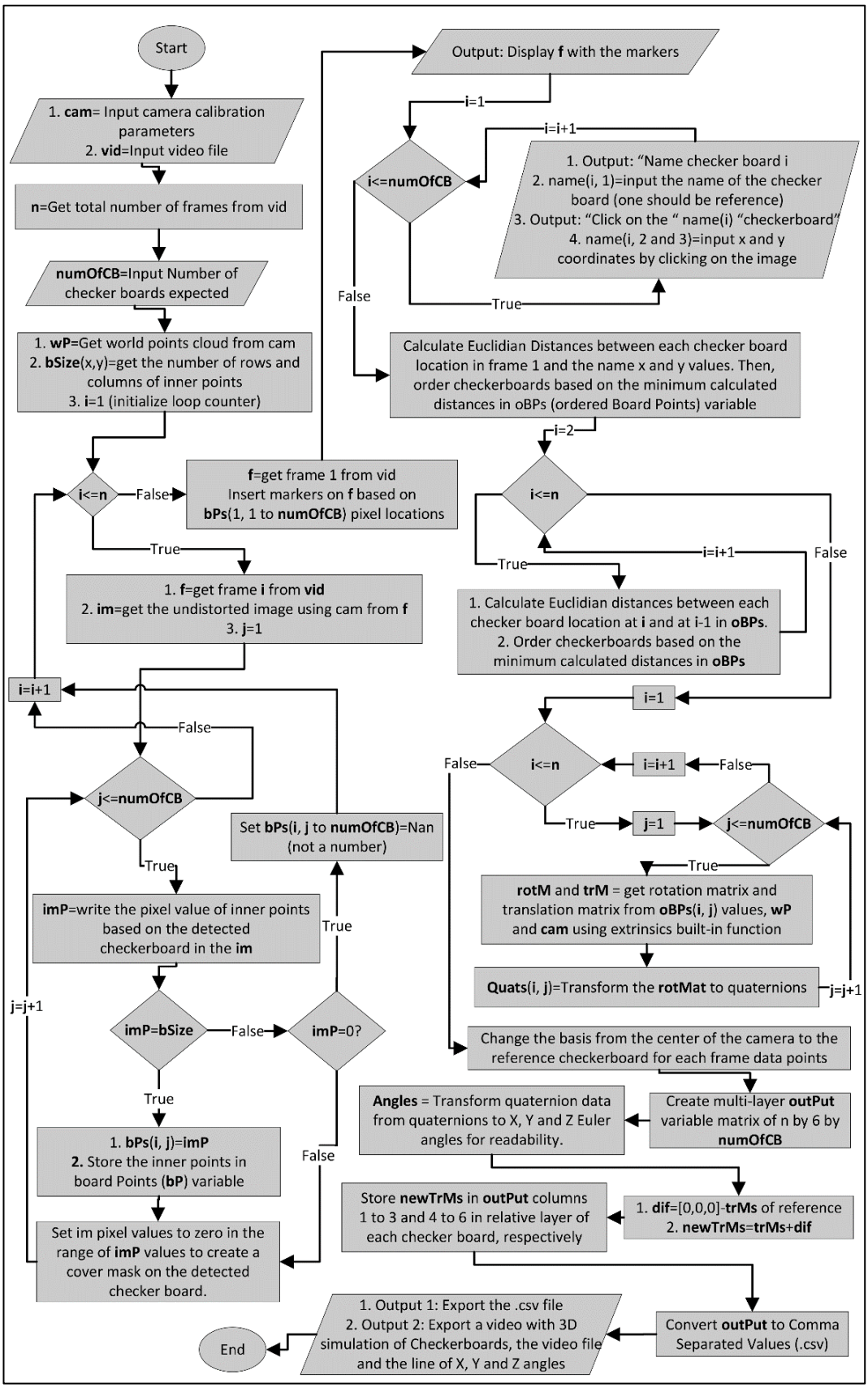

Appendix B: Histograms for Location Error of Pattern

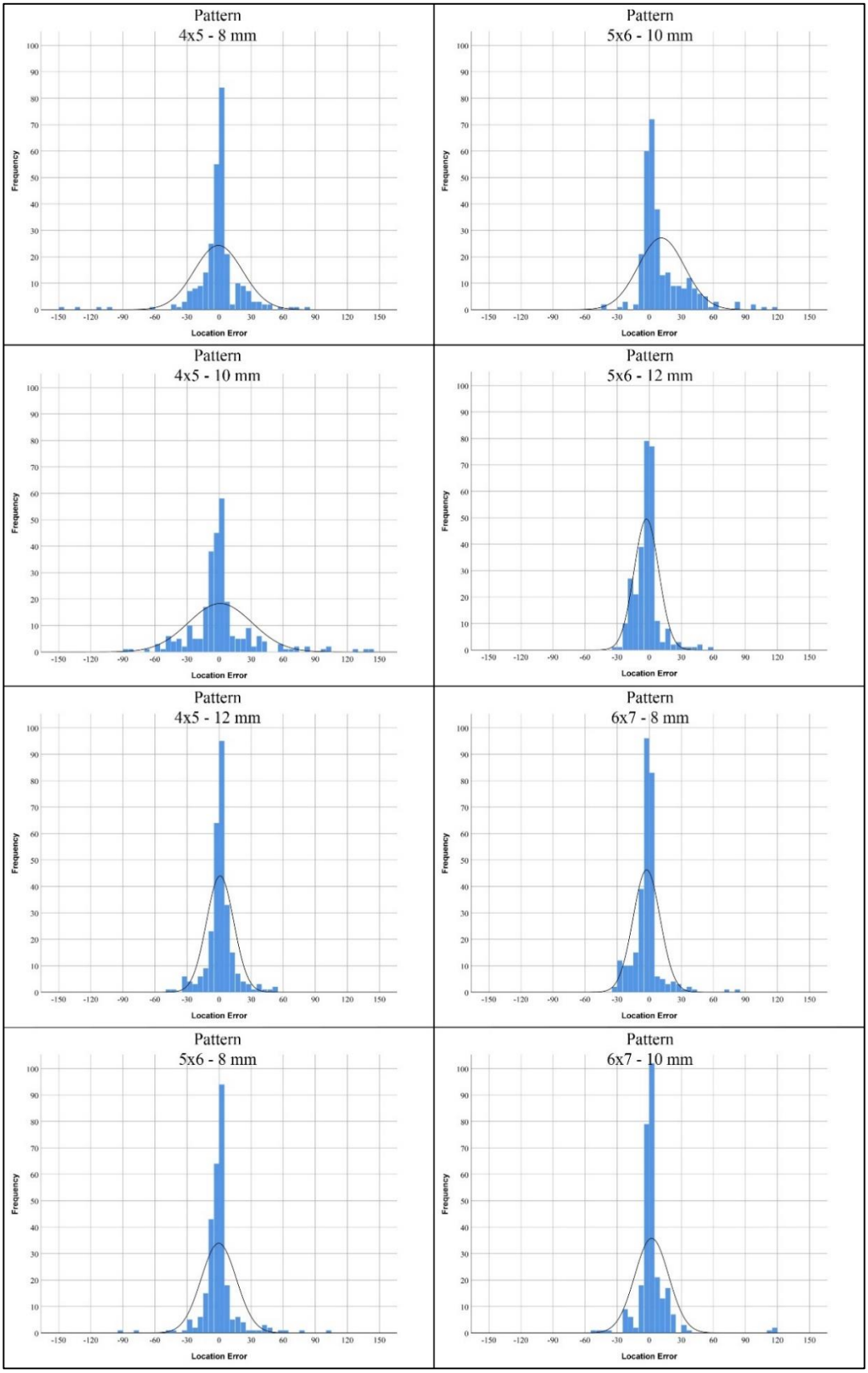

Appendix C: Histograms for Orientation Error of Pattern

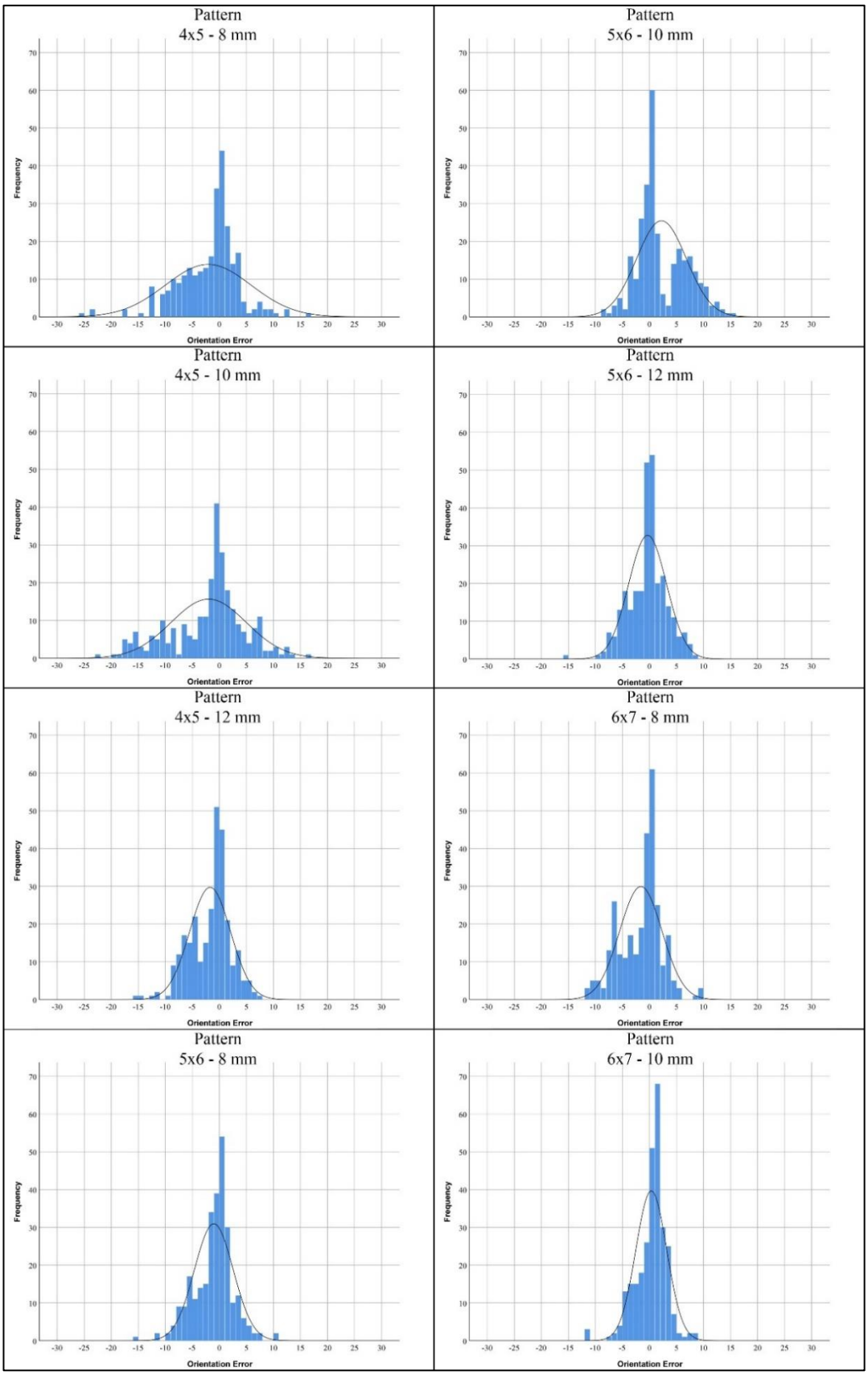

Appendix D: Histograms for Error of Resolution

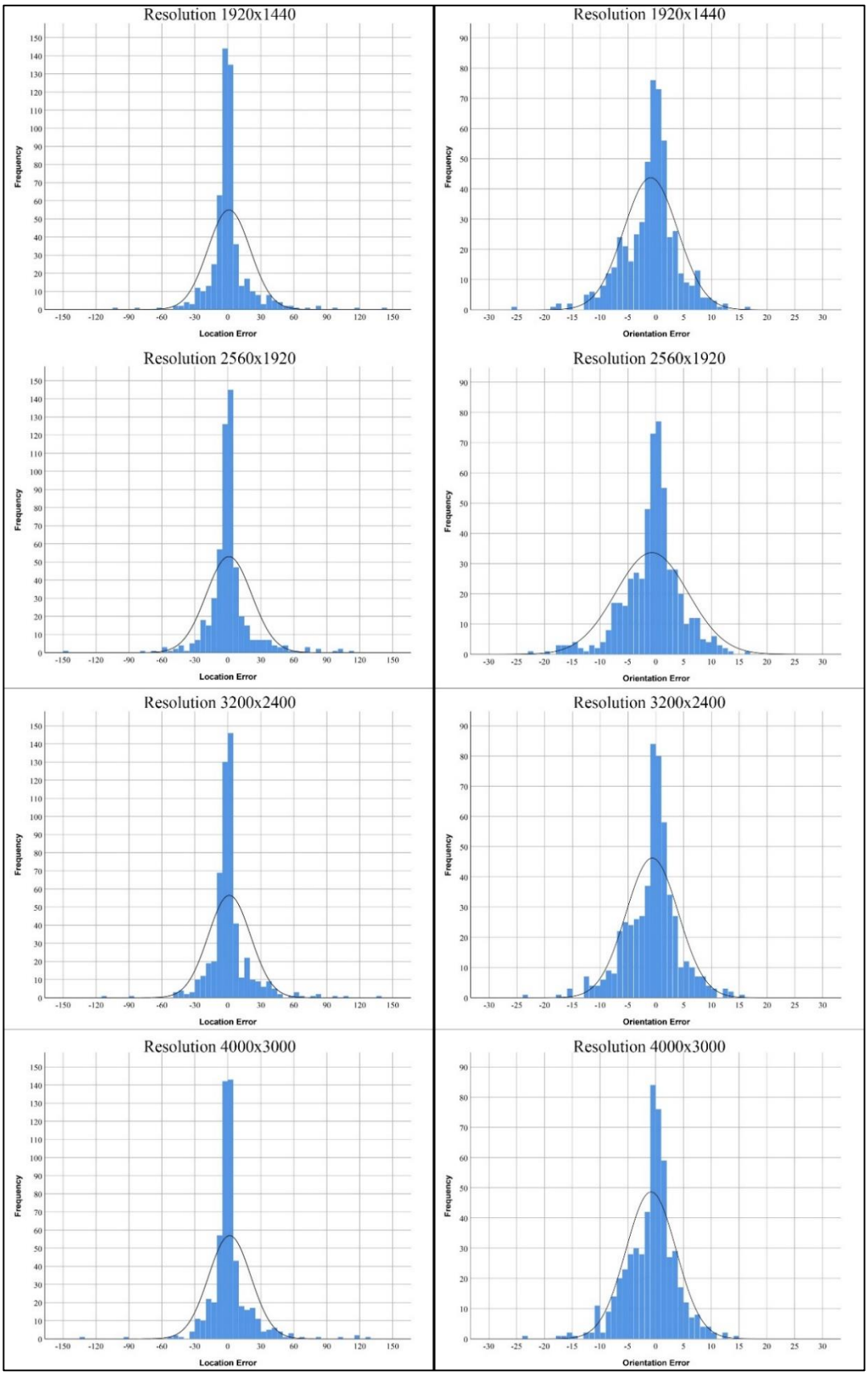

Appendix E: Histograms for Error of Axes